Making *in vivo* models viable again:

Synthetic lethality between DNA repair factors Xlf and Paxx is rescued by inactivation of Trp53

Sergio Miguel Castaneda Zegarra

This thesis is submitted in partial fulfilment of the requirements for the degree of Master of Science in Biomedical Sciences

Department of Biomedicine

Faculty of Medicine

University of Bergen

Spring 2019

Acknowledgements

This project was conducted in the laboratory of Dr. Valentyn Oksenych, leader of the Non-Homologous End-Joining group at the Faculty of Medicine and Health Sciences, NTNU as part of my MSc in Biomedical Sciences (Department of Biomedicine, Faculty of Medicine, University of Bergen).

First, I would like to thank my main supervisor, Dr. Valentyn Oksenych, for his great supervision and extraordinary guidance during all this time. For being more than just an advisor, for letting me improve every day as a scientist and as a person.

Second, I would like to thank all members of our group and others working in the lab. Thank you for helping me out whenever I needed it and working as a team. Really, it was a pleasure to work with you, Mengtan Xing, Camilla Huse, Øystein Røsand and Carole Beck. Thanks Raquel Gago-Fuentes even though we did not spend so much time working together, however, your initial help was fundamental.

I would like to thank Bjørnar Sporsheim from the Molecular Imaging Core (CMIC) at the Faculty of Medicine and Health Sciences – NTNU, for his time and help during my training to get microscope images. At the same time, I would like to thank my internal supervisor, Nils Halberg from UiB.

To my beautiful family, for the strength, love, and understanding that unites us every day, for you, I will fight to achieve each one of my dreams. Finally, I would like to thank especially my brother, Giancarlo, mainly because all these achievements would be impossible without his support.

Table of contents

LIST OF FIGURES

LIST OF TABLES

ABBREVIATIONS

A-NHEJ	Alternative Non-Homologous End-Joining
Ag	Antigen
B-mat	Mature B cell
BCR	B Cell Receptor
bp	Base pair
BSA	Bovine Serum Albumin
C-NHEJ	Classical Non-Homologous End-Joining
CCD	Charge-coupled device
CD	Cluster of Differentiation
CSR	Class Switch Recombination
D	Diversity
DDR	DNA Damage Response
dH_2O	Distilled water
DMEM	Dulbecco's Modified Eagle Medium
DN	Double Negative
DNA	Deoxyribonucleic acid
DNA-PKcs	DNA-dependent Protein Kinase catalytic subunit
DP	Double Positive
DSB	Double-Strand Break
DTT	Dithiothreitol
EDTA	Ethylenediaminetetraacetic acid
FBS	Fetal Bovine Serum
HRP	Horseradish Peroxidase
G0	Resting phase cell cycle
G1	First gap phase **c**ell cycle
G2	Second gap phase **c**ell cycle
H	Heavy chain
HR	Homologous Recombination
HSC	Hematopoietic stem cells
Ig	Immunoglobulin

IR	Ionizing radiation
J	Joining
kDa	Kilodalton
Ku	Ku70/Ku80 heterodimer
L	Light chain
Lig4	DNA Ligase IV
M	Mitosis phase
Min	Minute
MRI	Modulator of retroviral infection
Mut	Mutant
NHEJ	Non-Homologous End-Joining
Osc	Oscillation
PAXX	Paralogue of XRCC4 and XLF
PBS	Phosphate-Buffered Saline
PBS-T	Phosphate-Buffered Saline – Tween 0.1%
PCR	Polymerase Chain Reaction
Pre-T	T-cell precursors
Pro-B	Progenitor B cells
RAG1	Recombination Activating Gene 1
RAG2	Recombination Activating Gene 2
RBC	Red Blood Cell
RPM	Revolutions per minute
RSS	Recombination signal sequence
RT	Room temperature
S	Synthesis phase
SCID	Severe Combined Immunodeficiency
SP	Single positive
SSB	Single-Strand Break
T-mat	Mature T cell
TBE	Tris-Borate-EDTA
T_C	T Cytotoxic Cell
TCR	T Cell Receptor

TF	Tail fibroblasts
T_H	T Helper cell
Trp53	Transformation related protein 53
V	Variable
V/V	Concentration in volume/volume
V(D)J	Variable(Diversity)Joining
WT	Wild Type
WB	Western blot
XLF	XRCC4-Like Factor
XRCC4	X-ray Repair Cross-Complementing protein 4

SUMMARY

Non-Homologous End-Joining (NHEJ) is the major DNA repair pathway that senses, processes and ligates DNA double strand breaks (DSBs) in higher eukaryotes, functionally throughout the cell cycle. The NHEJ involves four core and some accessory factors. The accessory factors are mainly required for resolving specific types of lesions. During NHEJ, core Ku70 and Ku80 subunits bind DSBs as a heterodimer and promote further recruitment of accessory factors (e.g., XLF, PAXX, MRI, DNA-PKcs, Artemis) and downstream core subunits XRCC4 and DNA ligase 4 (Lig4). Paralogue of XRCC4 and XLF (PAXX) has shown to be redundant with the XRCC4-Like Factor (XLF).

Inactivation of *Ku70* or *Ku80* genes in mice results in immunodeficiency and high levels of genomic instability. While knockout of individual *Xlf* or *Paxx* in previously published mouse models revealed no overt phenotype, combined *Xlf* and *Paxx* deficiency results in late embryonic lethality (E15.5) due to extensive apoptosis in the central nervous system. These findings indicate important overlapping functions among the two proteins.

The first aim of this project was to investigate if the lethality of $Xlf^{-/-}Paxx^{-/-}$ mice can be rescued by inactivating one or two alleles of *Trp53*. This was done by crossbreeding $Xlf^{+/-}Paxx^{+/-}Trp53^{+/-}$ mice and verified by gene and protein expression.

The second aim of this project was to describe the impact of *Xlf* and *Paxx* in immune system and general mouse development. Our $Xlf^{-/-}Paxx^{-/-}$ mice with deficiency for one or two alleles of *Trp53* were here found to be distinguishable from single knockout $Xlf^{-/-}$ and $Paxx^{-/-}$ and heterozygous mice in relation to growth and lymphoid cell counts in the spleen and thymus. B and T cell frequencies in the spleen and thymus of $Xlf^{-/-}Paxx^{-/-}Trp53^{+/-}$ mice were evaluated in order to determine precisely the effect of *Xlf* and *Paxx* inactivation on lymphocyte development. I detected no B cells in the spleens and thymi of double knockout mice. However, I detected $CD4^+$ and $CD8^+$ T cells in both organs, in addition to nearly normal $CD4^+CD8^+$ T cell frequency. Furthermore, $Xlf^{-/-}Paxx^{-/-}Trp53^{+/-}$ TFs were evaluated every 48 hours until the sixth day in order to identify the proliferative power of $Xlf^{-/-}Paxx^{-/-}$ cells. $Xlf^{-/-}Paxx^{-/-}Trp53^{+/-}$ TFs showed a significantly reduced proliferation compared to heterozygous and single knockout controls.

Additionally, an optimization of the T-FISH technique was established in order to identify genomic instability at the chromosomal level. Some technical improvements in the assay allowed me to identify that *Xlf*$^{-/-}$*Paxx*$^{-/-}$*Trp53*$^{+/-}$ mice possess high numbers of chromosomal/chromatid breaks compared to heterozygous and single knockout controls. However, the small number of used samples did not allow me to make a solid conclusion and more mice are required to complete the study.

In conclusion, I demonstrated that inactivation of pro-apoptotic factor *Trp53* rescues embryonic lethality of *Xlf*$^{-/-}$*Paxx*$^{-/-}$ double knockout mice.

1. INTRODUCTION

1.1 The Immune System

The immune system has as a major task to protect the individuals from environmental agents, such as microbes or chemicals, preserving the integrity of the host [1]. However, it has other relevant functions as well, like the following ones [2]:

1. Memory function, providing long-lasting security against infection.

2. It does not attack its own tissues or put its beneficial cohabitants in jeopardy.

Furthermore, the immune system, depending on the specificity and speed of the required reaction activates two classes of responses, innate and adaptive responses, even though, the interaction between them is high[3].

The innate immune system provides immediate host defense and is highly conserved evolutionarily. It consists of physical, chemical and microbiological barriers. Moreover, the innate immunity includes characteristic elements, such as macrophages, neutrophils, monocytes, and cytokines, among others. Nevertheless, the reactions carried out by this immune system can cause damages and injuries to normal tissues given the lack of specificity[4].

On the other hand, the second class of immunity is highlighted for being present in higher animals and human beings. Adaptive response can take from days to weeks; however, they are accurate because of the antigen specificity carried out by B and T lymphocytes. One of the major responses long-term is the lymphocytic memory; allowing rapid and effective responses to repeated exposures [5].

Furthermore, the immune system organs are divided in two groups, primary and secondary immune organs. The primary organs of the immune system include the thymus and bone marrow, while the secondary lymphatic tissues include spleen, tonsils, lymph vessels, lymph nodes, adenoids, skin, and liver[6].

1.2 The adaptive immune system and lymphocyte development

The adaptive immune system is highly regulated by the interaction between antigen-presenting cells and the B and T lymphocytes. This system protects the host through several characteristics such as immunologic memory, specific effector pathways and regulation of the homeostasis [7, 8]. B and T lymphocytes are derived from specific types of stem cells called hematopoietic stem cells (HSCs) in the bone marrow. Developing B cells pass through several stages in order to acquire their antigen specificity in the absence of any exogenous antigen [9, 10]. Differently, T cells develop in the thymus, another primary immune organ [11, 12] (Figure 1).

Development and activation of B and T lymphocytes depends on a process which involves genetic rearrangement in the *variable (V)*, *diversity (D)* and *joining (J)* gene segments, known as V(D)J recombination. V(D)J recombination leads to the enormous repertoire of B and T cell receptors, that are able to recognize specific antigens[7].

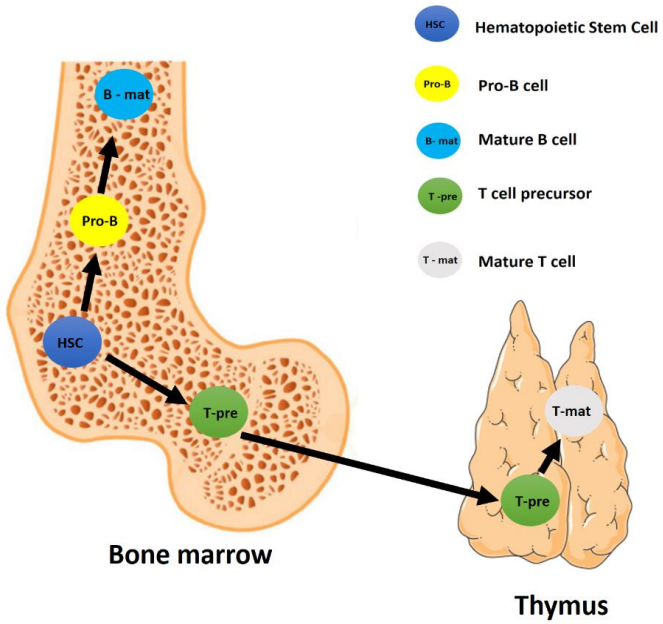

Figure 1: Simplified overview of B and T lymphocyte development. Hematopoeitic stem cells (HSCs) further develop to T cell precursors and Pro-B cells. Pro-B cells maturate to B cells after successful V(D)J recombination, dependent on the NHEJ. T-pre cells migrate to thymus and maturate to T cells. * Cell subset explanation is provided in the sections 1.2.2 and 1.2.3. Image inspired from the book by Kindt Thomas, Goldsby Richard and Osborne Barbara. *Kuby Immunology, sixth edition*, New York, USA. W.H Freeman and Company[6].

1.2.1 V(D)J Recombination

V(D)J recombination is a physiological mechanism which is fundamental for the development and maturation of B and T cells. V(D)J recombination requires DNA double strand breaks (DSBs) to trigger the recombination. This process involves the generation of different combinations of the V(D)J pre-existing gene segments. This pathway includes cleavage within specific recombination signal sequence (RSS) by the recombination activating gene 1 and 2 proteins (RAG1 and RAG2), operating as a complex called RAG. The V(D)J recombination preferentially occurs in the first gap phase (G1) of the cell cycle, because RAG2 protein is 20-fold more abundant in G1 phase than in the mitosis (M), second gap phase (G2) or synthesis phase (S) of the cell cycle in both precursors of B or T lymphocytes[13].

The RSSs are composed of three elements; a heptamer of seven conserved nucleotides, a spacer region of 12 or 23 base pairs, and a nonamer of nine conserved nucleotides. Initially, RSSs flank the *V*, *D* and *J* gene segments then; the segments are rearranged next to each other during the resolution of these DSBs. Consequently, they are rejoined, almost exclusively by the classical-NHEJ factors (explained in the section 1.3.2) resulting in a *V(D)J* gene segment[14, 15](Figure 2).

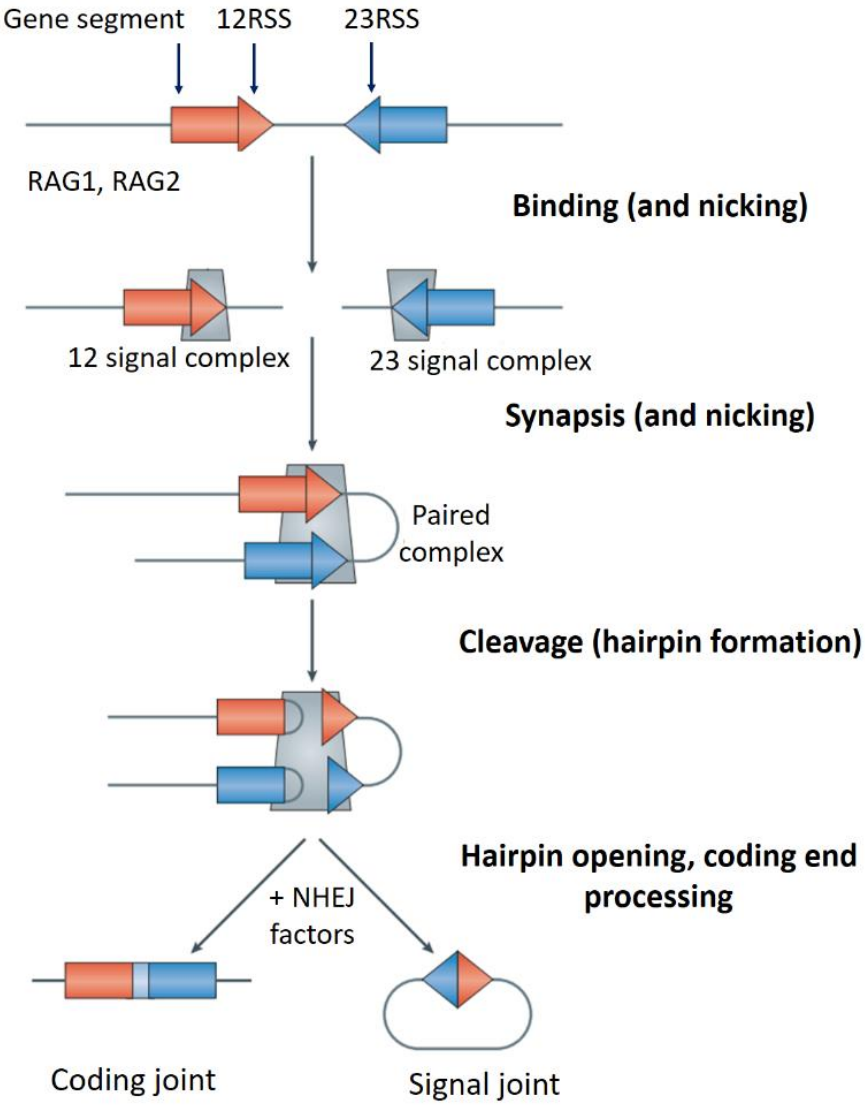

Figure 2: Simplified overview of V(D)J recombination. Gene segments are flanked by a 12 or 23 RSS recombination signal sequence (12 or 23 RSS). RAG1 and RAG2 proteins bind to the 12 RSS and the 23 RSS, forming the 12 signal complex or the 23 signal complex, respectively. Capture of the second RSS (a process termed synapsis) results in the formation of the paired complex, within which the RAG proteins introduce double strand breaks between the gene segments and the RSSs. Then, the non-homologous end joining (NHEJ) DNA repair factors rejoin the DNA ends into a coding joint. RSS ends are joined without processing to form the signal joint. Figure based on *Schatz, D. G., & Ji, Y. (2011). Recombination centres and the orchestration of V (D) J recombination. Nature reviews immunology, 11(4), 251.[16]*.

1.2.2 B cells

The B-cell development, both in humans and mice involves genetic rearrangements by acquiring antigenic specificity. Initially, the development of B cells begins in the fetal liver and continues in the bone marrow throughout our lives[17]. B cell development results in the production of a diverse collection of functional B-cell receptors (BCR)[18, 19].

The BCR is composed of two heavy (H) chains and two light (L) chains, κ or λ. The development of the BCR includes rearrangement of the *V*, *D*, and *J* gene segments in the H chain locus and the *V* and *J* gene segments in the L chain loci[10] (Figure 3). BCRs play role in the B-cell development, survival, and activation of B cells.

The BCR formation occurs in three developmental stages, pro-B, pre-B and immature B stage. Progenitor B (pro-B) cells develop to Pre-B cells, and the latter express pre-BCR. When the BCR process finishes (expressing cytoplasmic μH chains, also called immunoglobulin M (IgM)), B cells are immature and ready to interact with antigens (Ag) and become mature-B cells (Figure 4). The B-cell activation induced by Ag is carried out in secondary lymphoid tissues, for example in the spleen. A process called class switch recombination (CSR), or isotype-switching, leads to changes in the H chains, for instance, from IgM to IgA, IgE or IgG, giving rise to different effector functions depending on the recognized Ag [20].

Through the development of B cells, the different stages express co-receptors, such as CD43 and B220. However, CD19, a transmembrane glycoprotein, is the co-receptor expressed in almost all B cell stages (Figure 4) except for the differentiated plasma B cells, secreting antibodies[21].

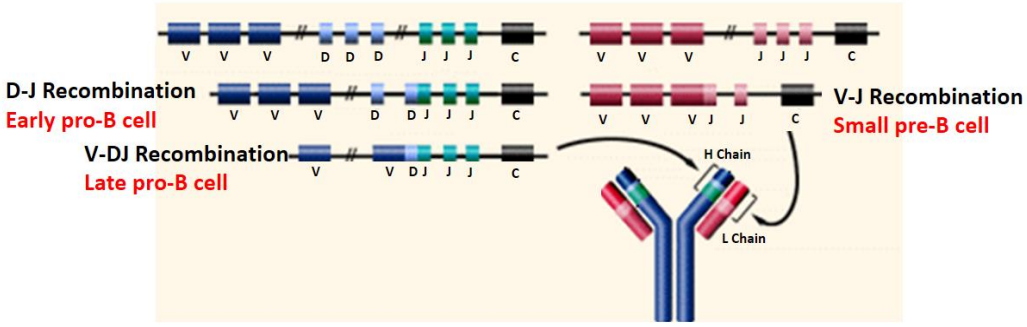

Figure 3: V(D)J recombination in B cells. The B cell receptor (BCR) is composed of two heavy chains (blue) and two light chains (red). In heavy chains the *D-J* recombination takes place in early pro-B cells followed by *V-DJ* recombination in late pro-B cells. In light chains *V-J* recombination occurs in small pre-B cells. *V*: Variable gene segments, *D*: diversity segments, *J*: joining segments and *C*: Constant *Igh* gene region. Figure modified from the book by Peter Parham. *The Immune System, third edition.* Garland Science*[22]*.

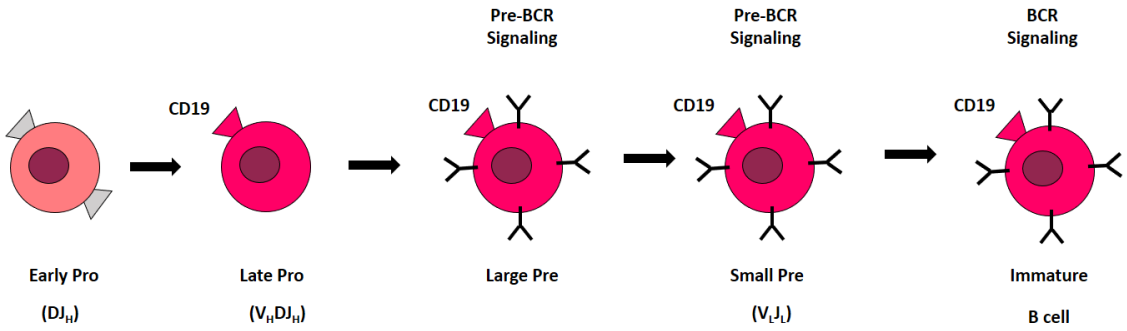

Figure 4: B-cell development from early pro-B cells to immature B cells. Formation of BCR signaling by V(D)J recombination. Rearrangements of the *D* and *J* gene segments in the immunoglobulin heavy chains occurs in early pro-B cells, followed by *V* segment rearrangement in the late pro-B cells forming the Pre-BCR on large pre-B cells. The last rearrangement takes place in small pre-B cells in the *V* and *J* segments producing the BCR signaling on immature B cells. CD19 is a co-receptor expressed on late pro-B cells, large pre-B cells, small pre-B cells and immature B cells. Figure inspired from *Holmes, M. L., Pridans, C., & Nutt, S. L. (2008). The regulation of the B-cell gene expression programme by Pax5. Immunology and cell biology, 86(1), 47-53*[23].

1.2.3 T cells

Hematopoietic stem cells in the bone marrow originate T-cell precursors (T-pre cells), which develop to T cells. T-pre cells migrate and colonize the thymus. In the thymus, the precursors of T cells undergo a developmental process with the purpose to maturate and express the T cell receptor (TCR). Approximately 95 % of the T cells in the thymus give rise to αβ T cells, however approximately 5% will express the γδ T cell receptor (TCR) (Figure 5). *V, D* and *J* variable gene segments are assembled into the β and δ receptor chains, whereas the α and γ receptor chains are constituted of V and J variable regions[6].

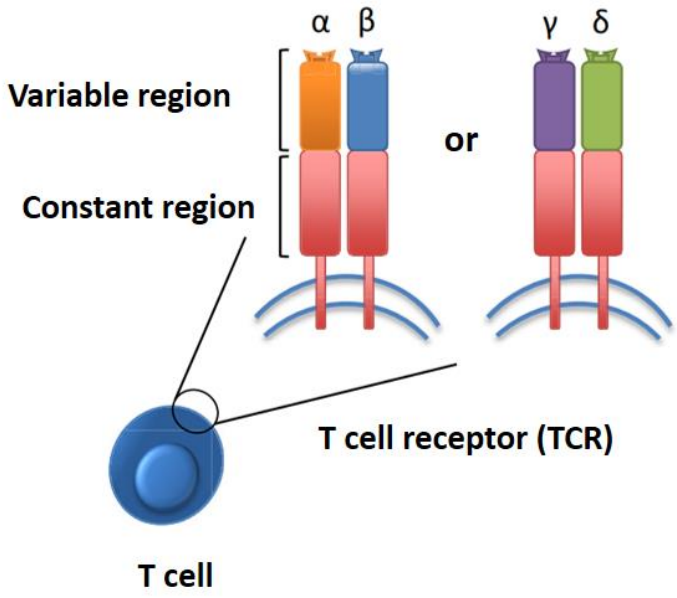

Figure 5: The T cell receptor (TCR) is composed of a combination of α and β chains or γ and δ chains in the variable region of the receptor. Constant regions are identical in both kinds of receptors. Figure modified from *Matos, T. R., de Rie, M. A., & Teunissen, M. B. (2017). Research techniques made simple: high-throughput sequencing of the T-cell receptor. Journal of Investigative Dermatology, 137(6), e131-e138[24]*.

T-cell precursors give rise to double negative (DN) cells; DN cells lack expression of the co-receptors CD4 and CD8. The DN T cells can be sub-divided into four subsets (DN1-4). DN T population is characterized according to the expression of receptors such as c-kit (a receptor tyrosine kinase), CD44 (an adhesion molecule) and CD25 (Interleukin-2 receptor α chain). The Figure 6 shows the ordered expression of these markers in the four types of DN T cells[6].

V(D)J rearrangement is initiated in DN2 T cells, specifically in the β chain locus culminating in DN3 T cells. The latest cells undergo a process called beta-selection. This process of selection allows an accurate and successful rearrangement in the TCR-β chain locus. The β chain pairs with the surrogate chain, pre-Tα, producing a pre-TCR, which forms a complex with the protein complex CD3. Cells that do not endure beta-selection die via apoptosis. When β-chain rearrangement is completed, DN3 T cells turn into DN4, leading to the survival, proliferation, and further differentiation in double positive (DP) cells by up-regulation and expression of CD4 and CD8. Immediately, DP cells stop proliferating, and start the rearrangement of the V and J segments in the α chain locus, increasing the protein levels of RAG-2, which is essential for the maturation of T lymphocytes. Moreover, RAG-2 is regulated by phosphorylation to induce its degradation upon entry S phase [25]. DP T cells maturate into single positives (SP) $CD4^+$ (T helper – T_H) or $CD8^+$ (T cytotoxic or T_C) T cells depending on the different cell interactions. The T_H and T_C activate B cells and lyse infected target cells, respectively[6, 26] .

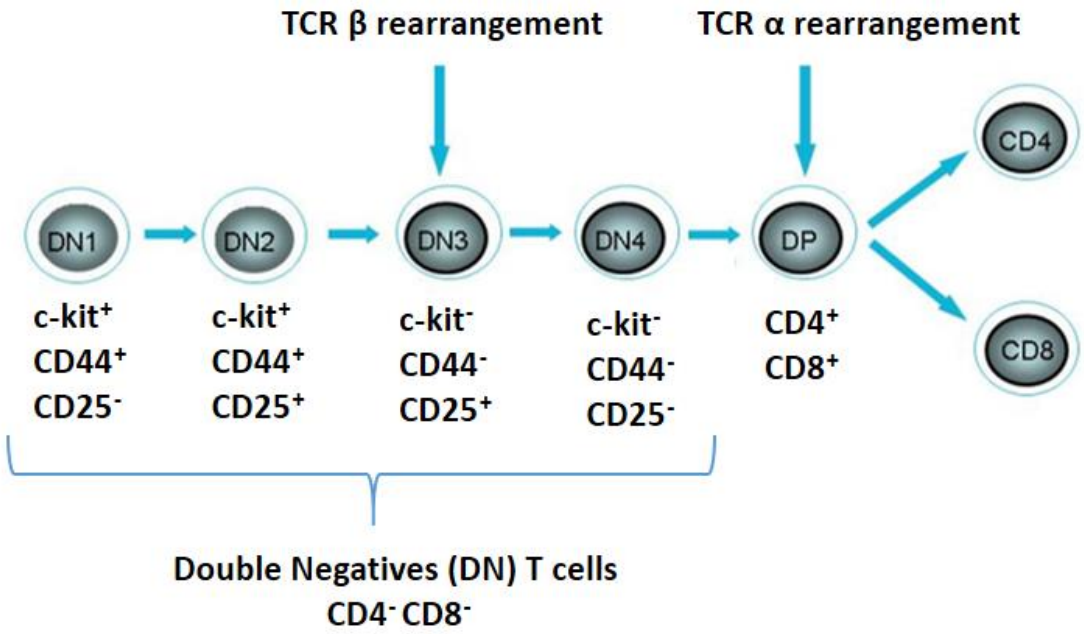

Figure 6: Development of T cells from double negative (DN) cells to $CD4^+$ or $CD8^+$ T cells in the thymus, showing αβ T cell development and the different cell surface markers expressed at the different stages of T cell maturation in mice. Figure modified from *Divya K. Shah, Sunnybrook Research Institute, Toronto Canada. T-cell development in thymus. British Society for Immunology* [26].

1.2.4 Lymphoid Cell Frequencies

The process of B and T cell maturation takes places in the primary immune organs, bone marrow and thymus, respectively. However, the activation of B-lymphocytes occurs in the spleen, a secondary lymphoid organ.

By flow cytometry, it has been possible to identify the distinct cell types which reside both in the spleen and thymus. In the spleen, there are mainly red blood cells (RBC), B cells, $CD4^+$ T cells (T_H) and $CD8^+$ T cells (T_C). Moreover, in the thymus there are both immature $CD4^+CD8^+$ T cells and mature T cells ($CD4^+$ or $CD8^+$) [27]. The Table 1 shows the expected frequencies of B and T lymphocytes both in the spleen and thymus in mice.

Table 1: Expected B and T cell frequencies (%) in the spleen and thymus of adult mouse. Table based on *Bio-rad*. Flow Cytometry – Cell frequency.2017[27]

Spleen		**Thymus**	
Cell type	**Percent %**	**Cell type**	**Percent %**
T cells	21 - 35	$CD4^+$	4 - 6
$CD4^+$	13 - 20	$CD8^+$	1 - 2
$CD8^+$	7 - 15	$CD4^+$ $CD8^+$	85 - 95
B cells	44 - 58	-	-

1.3 DNA Repair

DNA repair maintains the genomic stability, preventing an uncontrolled cellular death, premature cell aging, degenerative changes, chromosomal aberrations and immunodeficiency. However, endogenous and exogenous agents constantly damage the primary structure of the DNA, giving rise to simple and complex changes in the DNA, from base changes to chromosomal aberrations, thus an accurate DNA repair is necessary for homeostasis [28].

Depending of the agent nature, the DNA damages can cause single-strand breaks (SSBs) or double-strand breaks (DSBs). Nevertheless, several strategies are utilized for its recognition by activating particular DNA repair pathways with the aim to trigger proper responses [29, 30].

1.3.1 DNA Double-Strand Breaks (DSBs)

DSBs are one of the most lethal type and deleterious forms of DNA damage. They can be originated in response by both exogenous and endogenous agents[31]. DBSs are produced physiologically through normal processes both in developing lymphocytes (B and T cells) by V(D)J recombination and in mature B cells by immunoglobulin class-switching. Furthermore, the repair of DSBs in eukaryotic cells is carried out by two main pathways, non-homologous end joining (NHEJ) and homologous recombination (HR)[32, 33].

NHEJ is the major mammalian DSB repair pathway, which is active throughout the whole cell cycle, especially in the G1 of the cell cycle. Meanwhile, HR is the main DSB repair pathway used during the S and the G2 phases when sister chromatids are available and intact. Therefore, the cell chooses which pathway is better to repair DSBs depending on the phase of the cell cycle where cell is present [31, 34] .

1.3.2 Non-Homologous End-Joining (NHEJ)

NHEJ consists of both the classical-NHEJ (C-NHEJ) and the alternative-NHEJ (A-NHEJ) pathways. NHEJ is the major system to repair DSBs in higher eukaryotes and is active during all phases of the cell cycle, being most important during the G1 phase [34]. This pathway is formed by the core and accessory factors to repair DSBs. The core factors are also called essential factors, and are made up of four proteins, Ku70, Ku80, X-ray repair cross-complementing protein 4 (XRCC4), and DNA ligase IV (LIG4); the first two proteins form the heterodimer Ku70/Ku80 (Ku). The accessory NHEJ factors include DNA-dependent protein kinase catalytic subunit (DNA-PKcs), Artemis (an essential nuclease during V(D)J recombination in lymphocytes), XRCC4-like factor (XLF/Cernunnos, sometimes also regarded as core factor), Paralogue of XRCC4 and XLF (PAXX/XLS), and Modulator of retroviral infection (MRI/Cyren)[30, 35] (Figure 7). C-NHEJ pathway can be divided to three distinct stages. First, the recognition of the DSBs; second, the processing to remove overhangs and hairpins; and third, a DNA ligation.

Initially, the Ku heterodimer binds the DSBs acting as a DNA damage sensor and stabilizing the DNA ends [36]. In addition, Ku inhibits alternative DNA repair pathways such as HR and A-NHEJ [37]. Furthermore, Ku recruits and activates DNA-PKcs forming a holoenzyme (DNA-PK). DNA-PKcs auto-phosphorylates itself and phosphorylates other C-NHEJ factors [38, 39]. PAXX binds and stabilizes the Ku complex [40]. Finally, XLF interacts both with Ku and the XRCC4–LIG4 complex stimulating DNA ligation [41, 42]. In patients, it has been reported that a partial loss of NHEJ genes is characterized by microcephaly, immunodeficiency and, cancer susceptibility [43-46].

A-NHEJ also repairs double-strand breaks, however, it is characterized by microhomology-mediated ligation with length of homology regions ranging from 1 to 25 base pairs (bp). Unlike C-NHEJ, A-NHEJ relies on other factors and its composition is not fully understood yet [47]. Usually, A-NHEJ is associated with chromosome abnormalities such as deletions, translocations and inversions [48]. However, the high abundance of Ku in cells increases the likelihood that Ku is the first protein to bind to a broken DNA ends and, by consequence, the DNA repair is more often carried out through the classical NHEJ pathway[49].

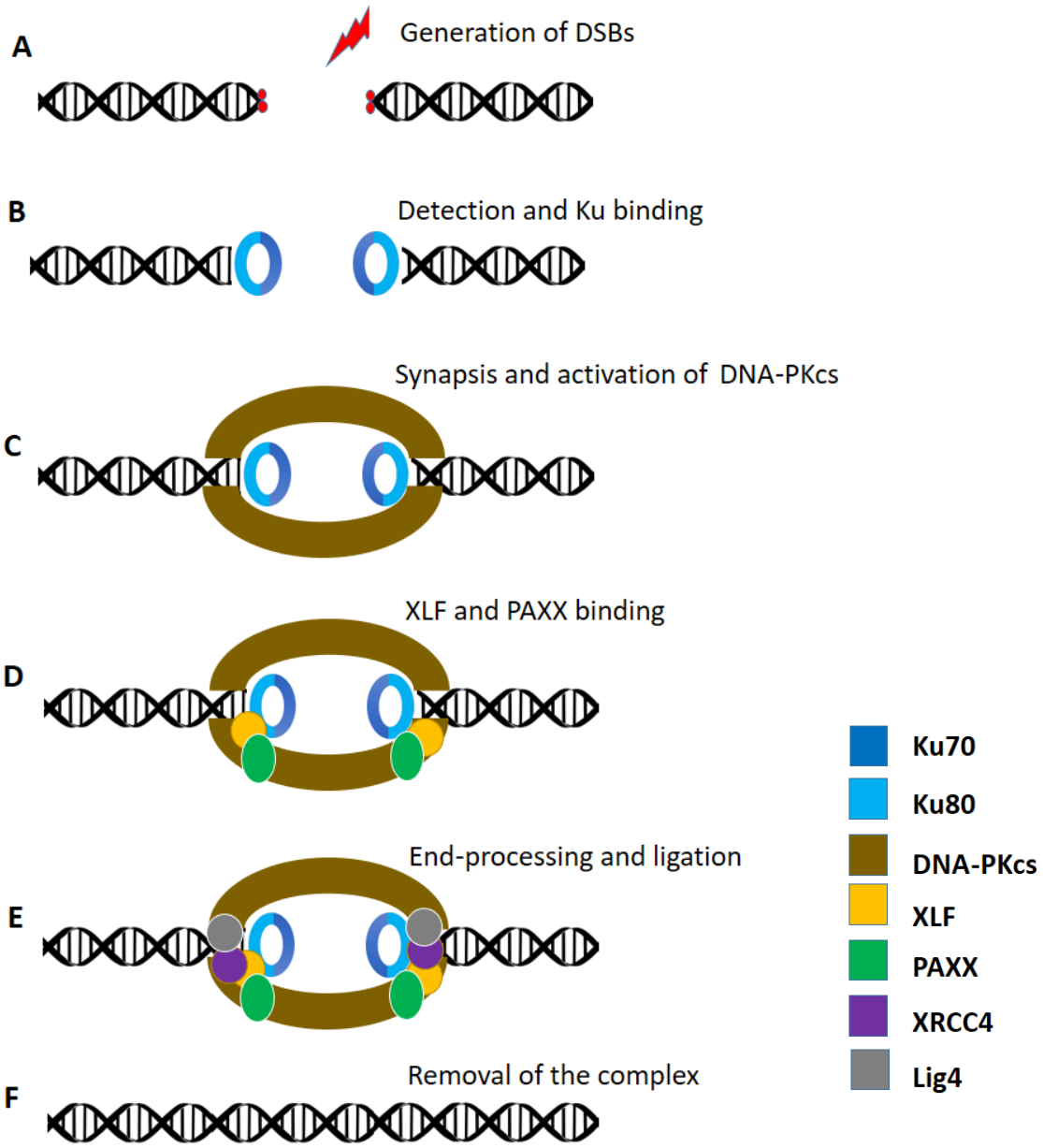

Figure 7: Simplified overview of the NHEJ pathway. **A)** DNA double strand breaks caused by genotoxic factors. Chemically modified DNA ends (red circles) are ready to be processed. **B)** Ku heterodimer (Ku70/Ku80) recognizes and binds tightly to both DNA ends. **C)** Ku recruits DNA-PKcs forming a synapse between the DNA ends. **D)** Stabilization of the complex by binding of accessory factors XLF and PAXX. **E)** End-processing and ligation by XLF and two core factors, XRCC4 and LIG4. **F)** Removal of the protein complex. Ku70: blue, Ku80: light blue, DNA-PKcs: brown, XLF: yellow, PAXX: green, XRCC4: purple and Lig4: gray color. This figure is based on Rulten, S. L., & Grundy, G. J. (2017). *Non-homologous end joining: common interaction sites and exchange of multiple factors in the DNA repair process. Bioessays, 39(3), 1600209[50]*.

1.3.3 NHEJ factors: XLF and PAXX

In 2006, a scientific group reported five patients with mutations in a new protein, initially called *Cernnunos* or XLF, which resulted in a new syndrome associated with immunodeficiency, B and T lymphocytopenia, growth retardation, and microcephaly [43]. In addition, in the same year, another group discovered XLF as a NHEJ factor.

XLF interacts with the core factors XRCC4 and Lig4 during the DNA ligation [51]. Nevertheless, in a mouse model, the lack of XLF does not result in the same phenotype as in humans. In particular, the V(D)J recombination in B and T cells is carried out with wild type rates in the absence of XLF, moreover, mature lymphocyte number in XLF-deficient mice is only modestly decreased [52, 53].

In 2014-2015, three independent groups reported a new protein initially called C9orf142, XLS (XLF-like small protein), or PAXX (Paralogue of XRCC4 and XLF). The structural similarities between PAXX and XLF are shown in the Figure 8. However, regardless of the structural similarity, PAXX shares little sequence homology with XLF and XRCC4 [40, 54, 55]. During NHEJ, PAXX is rapidly recruited to the DNA damage sites, promotes the Ku binding at DNA ends by stabilizing the NHEJ machinery, and cooperates with XLF [40]. Despite that, PAXX does not interact directly with XLF or with the core factors XRCC4 and Lig4 [55, 56]. *Paxx* knockout mice showed to be fertile with a normal growth and a mild sensitivity to radiation [56-59].

Finally, XLF-deficient human patients possess extreme sensitivity to IR, microcephaly, and growth retardation, nevertheless, the effects are variable on the immune system [43, 60]. This year 2019, Recio, M., *et al.*, reported two unrelated cases diagnosed with the same non-sense mutation, but with significant differences in the immunological profile. The first patient showed a senescent phenotype and impaired T-cell development, whereas the second patient only had a slight reduction in T-cell counting [61]. Until now, there is no reported cases of PAXX-deficiency in humans, however, the patients with mutated PAXX might be identified in the future.

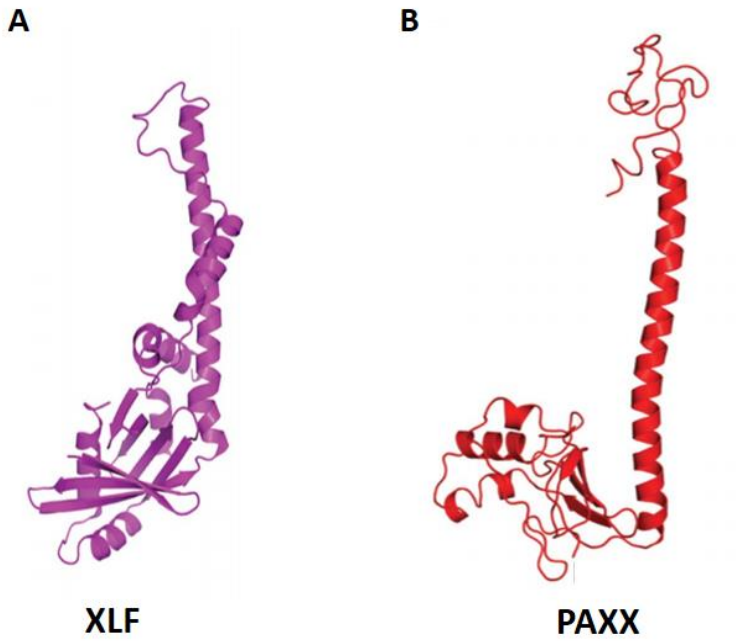

Figure 8: Simplified overview of the predicted crystal structures of XLF and PAXX. **A)** 3D structural model of PAXX (Paralogue of XRCC4 and XLF). **B)** 3D structural model for XLF. This figure is based on Craxton, A., et al. *"XLS (c9orf142) is a new component of mammalian DNA double-stranded break repair." Cell death and differentiation* 22.6 (2015): 890 *[54]*.

Mature B cell lacking XLF possess 2-3 fold reduction of CSR levels, while lack of PAXX had no effect on the CSR to IgA and IgG1 [53, 58, 62, 63]. Nevertheless, XLF and PAXX are functionally redundant during the V(D)J recombination in B and T lymphocytes[62, 64]. *In vitro* works reported that $Xlf^{-/-}$ $Paxx^{-/-}$ cells had more radiosensitivity compared to $Xlf^{-/-}$ and $Paxx^{-/-}$ cells. However, a double knockout of *Xlf* and *Paxx* in a mouse model was embryonically lethal due to increased apoptosis in central nervous system [56, 57, 59, 65]. This suggests that XLF and PAXX have overlapping functions.

1.3.4 Relation between p53 signaling and NHEJ factors

Tumor protein p53, also called transformation related protein 53 (Trp53) in mice has been described as "the guardian of the genome" because of its role in conserving genomic stability. Moreover, Trp53 senses and reacts to DNA damages through the ATM/ATR and Chk1/Chk2 kinases[66]. For example, ATM is activated in the presence of the DNA damage response (DDR), phosphorylates p53 and promotes the cell cycle arrest, apoptosis, and controls the proliferation of DNA damaged cells. If the DNA is repaired, the cells will go to S phase of the cell cycle. If the cells endure with DNA damage, they will undergo apoptosis mediated through the p53 pathway[67].

Deficiency for Ku70, Ku80, XLF, PAXX, DNA-PKcs, Artemis and MRI results in viable mice, while inactivation of XRCC4 or Lig4, as well as combined inactivation of XLF/PAXX, XLF/DNA-PKcs and XLF/MRI leads to late embryonic lethality likely due to severe apoptosis in the central nervous system [35, 53, 57, 68-74](Table 2).

However, inactivation of one or two alleles of p53 partially rescued this embryonic lethality [65, 71, 75, 76], highlighting the interaction between p53 and NHEJ during growth and development.

Table 2: Summary of *in vivo* NHEJ knockout models in mice, indicating viability. Additionally, it is mentioned if the absence of *Trp53* can partially rescue the lethality or not.

Knockout model	Viable	Viable when lacking *Trp53*
Ku70$^{-/-}$	Yes	
Ku80$^{-/-}$	Yes	
Xrcc4$^{-/-}$	No	Yes
Lig4$^{-/-}$	No	Yes
Xlf$^{-/-}$	Yes	
Paxx$^{-/-}$	Yes	
Dna-pkcs$^{-/-}$	Yes	
Mri$^{-/-}$	Yes	
Artemis$^{-/-}$	Yes	
Xlf$^{-/-}$ *Mri*$^{-/-}$	No	Unknown
Xlf$^{-/-}$ *Dna-pkcs*$^{-/-}$	No	Yes
Xlf$^{-/-}$ *Paxx*$^{-/-}$	No	Yes, this study

2. AIMS

Knocking out of one gene, *Xlf* or *Paxx* results in viable mice with modest or no phenotype, nevertheless, a combined deficiency for XLF/PAXX results in embryonic lethality due to extensive apoptosis in the central nervous system [56, 57, 59]. The lethality in mouse models lacking XRCC4, Lig4 or XLF/DNA-PKcs has been rescued by inactivating of one or two alleles of *Trp53* [71, 75, 76]. Therefore, the following objectives are proposed:

1. The first aim of this project is to investigate if the late embryonic lethality of $Xlf^{-/-}$ $Paxx^{-/-}$ mice can be partially or completely rescued by inactivating of one or two alleles of *Trp53*. This model allows studying XLF and PAXX double-deficiency *in vivo*.

2. If the absence of *Trp53* rescues the embryonic lethality of $Xlf^{-/-}Paxx^{-/-}$ mice, the second aim would be to characterize the model and the impact of combined *Xlf*/*Paxx*-inactivation on growth and immune system development *in vivo*. The following specific objectives are proposed:

    1. To analyze the lymphoid cell counts, weight of spleen, thymus and body, of $Xlf^{-/-}Paxx^{-/-}$ mice compared to WT, heterozygous and single-deficient controls.

    2. To determine the impact of combined *Xlf* and *Paxx*-inactivation on lymphocyte development, B and T cell frequencies in spleen and thymus, compared to WT, heterozygous and single knockout controls.

    3. To characterize the proliferative power of cells in the double deficient $Xlf^{-/-}$ $Paxx^{-/-}$ mice and controls.

    4. To optimize the Telomere Fluorescence in situ hybridization (T-FISH) technique and to investigate the genomic instability in double deficient and control cells at the chromosomal level.

3. MATERIALS AND METHODS

3.1 Mouse models

All experiments involving mice were performed according to the protocols approved by the Norwegian University of Science and Technology (NTNU). *Xlf*$^{+/-}$*[53]*, *Paxx*$^{+/-}$*[58]*, *Trp53*$^{+/-}$*[77]*, *Ku80*$^{+/-}$*[69]* and *Dna-pkcs*$^{+/-}$*[68]* mice were previously described. Primer sequences for genotyping and expected amplicons are provided in Appendix A.

3.2 Genotyping

3.2.1 DNA extraction and Polymerase Chain Reaction (PCR)

Ear-samples from mice were incubated overnight at 56°C with 2% Proteinase K solution (20 mg/mL) (Cat#AM2546, Ambion™) and 98% DNA lysis buffer (10mM Tris pH 9.0, 1M KCl, 0.4% NP-40, 0.1% Tween20) to extract DNA. Then, samples were incubated at 95°C for 30 minutes and centrifuged at 15 000 rpm for 15 minutes, and the DNA concentration was measured by a Nanodrop® ND-1000 Spectophotometer (Thermo Scientific, Waltham, Massachusetts, USA). Samples where diluted to get a final DNA concentration of approximately 50ng/µL. The PCRs were performed with 50ng DNA in a final reaction volume of 25µL, using the GoTaq® G2 Green Master Mix (Promega, Madison, USA). PCRs were run in a 2720 Thermal Cycler (Applied Biosystems™, Foster City, California, USA). PCR programs are provided in Appendix B.

3.2.2 Electrophoresis

Agarose gels with GelRed™ Nucleic Acid Gel Stain (diluted from 10 000x stock, Biotium, Fermont, California, USA) were prepared from 0.8% SeaKem® LE Agarose (Cat#50000, Lonza, USA) in Tris-Borate-EDTA (TBE) buffer (pH 8.4; 89mM Tris; 89mM Boric Acid; 2mM EDTA). Gel electrophoresis were run in TBE buffer at 124V for 75 minutes (100mL

gels), and the sample volume loaded was 10µL (~20ng DNA). For reliability, positive (WT sample), negative (knockout samples) controls and water were used in all assays. Quick-Load® 100bp DNA Ladder (Cat#N0467S, New England Biolabs® Inc.) and Orange G 5x ~50bp (15% glycerol; 0.2% Orange G dye, dH2O) were used as the ladder and tracking dyes, respectively. The gels were visualized and pictured with a Gel Logic 200 Imaging System (KODAK, USA).

3.3 Extraction and concentration of proteins

3.3.1 Protein extraction from cell culture

Samples from primary tail fibroblast cell culture were centrifuged at 1200 rpm for 5 minutes at 4°C. Pellets were gently re-suspended in 1mL of Phosphate-Buffered Saline (PBS) (Cat#10209252, Thermo Fisher Scientific) and centrifuged at 5000 rpm x 3 minutes x 4°C. Pellets were re-suspended in 96% of RIPA lysis buffer (Cat#R0278, Sigma Life Science) and 4% Complete EDTA-free Protease Inhibitor Cocktail diluted from 25x stock (Cat#P8340, Sigma-Aldrich) and incubated on ice for 30 minutes. Samples were centrifuged at 13000 rpms for 15 minutes at 4°C. Supernatants were collected and stored at -80°C.

3.3.2 Bradford curve and measurement of protein concentration

Protein concentration was determined by a Bradford assay, using Protein Assay Dye Reagent (Cat#5000002, Bio-Rad). The absorbance was measured at 595nm in a UV-1700 Spectrophotometer (Shimadzu, Kyoto, Japan). The final protein concentration was calculated and based on the standard curve of bovine serum albumin (BSA). Preparation of BSA standards and measured absorbance is presented in the Table 3 and 4, respectively. The BSA standard curve is presented in the Figure 9.

Table 3: Preparation of BSA standards. The Protein Assay Dye Reagent was diluted five times in dH2O prior to measurements. A stock solution of BSA (2µg/µL) was used.

	Standards					
	1	2	3	4	5	6
BSA (µg)/sample	0	2	4	10	14	22
Stock BSA (µL)	0	1	2	5	7	11
H_2O (µL)	20	19	18	15	13	9
5x diluted Protein Assay Dye Reagent (µL)	1000					

Table 4: Measured absorbance of BSA standards. The absorbance was measured at 595nm for BSA standards of 0, 2, 4, 10, 14 and 22µg.

	Standards					
BSA (µg)	0	2	4	10	14	22
A595nm	0	0,135	0,221	0,546	0,689	1,042

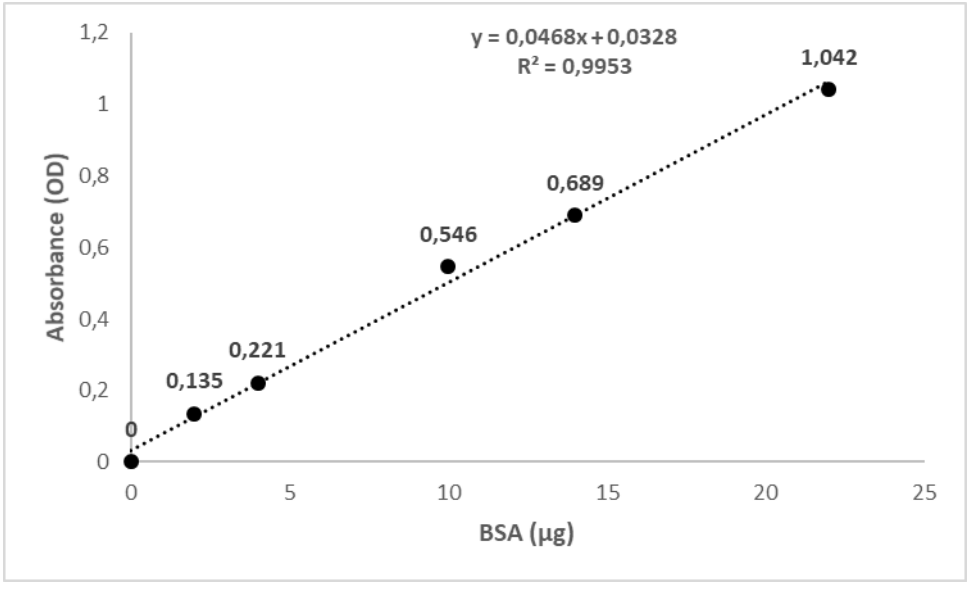

Figure 9: BSA standard curve. The equation, y = 0,0468x + 0,0328; R^2 = 0.9953, was used to estimate the protein concentration in cell lysates from tail fibroblasts.

In order to determine the concentration of my samples; the same protocol was followed but with 19µL dH2O, 1µL of sample, and 1000µL Protein Assay Dye Reagent (diluted 5x in dH_2O) mixed prior to absorbance measurements. The final protein concentration was calculated from the BSA standard curve.

3.4 Western blot

3.4.1 Electrophoresis

Western blots were prepared using around 50µg of protein samples and mixing them with NuPAGE® LDS Sample Buffer (originally 4x stock, Cat#NP0007, Invitrogen™) and 0.1M DTT (Cat#707265ML, Thermo Scientific), followed by an incubation of 10 minutes at 70°C. The samples were run in 4-12% Bis-Tris NuPAGE™ gels (Cat#NP0323, Thermo Fisher Scientific, Waltham, Massachusetts, USA) at 200V for 55 minutes in NuPAGE™ MOPS SDS Running Buffer (diluted from 20x stock, Cat#NP001, Thermo Fisher Scientific). MagicMark™ XP Western Protein Standard (Cat#LC5603, Invitrogen™) and SeeBlue™ Plus2 Pre-stained Protein Standard (Cat#LC5625, Invitrogen™) were used for molecular weight estimation and tracking during electrophoresis.

3.4.2 Electroblotting

Protein transfer was carried out on Amersham Hybond PDVF Blotting Membranes pore size 0.45µm (Cat#10600023, GE Healthcare Life Sciences, Marlborough, Massachusetts, USA). Wet electroblotting was run at 25V for 90 minutes in 10% Methanol NuPAGE™ Transfer Buffer (20x stock, Cat#NP0006, Invitrogen™) with NuPAGE™ Antioxidant (1000x stock, Cat#NP0005, Invitrogen™) at 4°C.

3.4.3 Chemoluminescence

Membranes were washed with PBS-Tween 0,1% (PBS-T) and blocked for 1 hour at room temperature (RT, ~22°C) in 5% milk (Non-fat dry milk, PBS-T), followed by an overnight incubation at 4°C with the primary antibody diluted in 5% milk. Next day, membranes were

washed three times for 5 minutes with PBS-T followed by 1h incubation with Horseradish Peroxidase (HRP)-conjugated secondary antibodies diluted in 5% milk. Membranes were washed again three times for 5 minutes with PBS-Tween 0,1%, and signals for protein bands were developed using a SuperSignal™ West Femto Maximum Sensitivity Substrate (Cat#34096, Thermo Scientific) in a ChemiDoc™ MP Imaging System (Cat#170-01402, Bio-Rad). All incubations and washings were done under agitation (20 osc/min). β-actin was used as loading control. Antibodies used in Western blots are described in the Table 5.

3.5 Cell Count in Lymphoid Organs

Initially, spleens and thymi were isolated from mice and collected in a tube with 0.5mL PBS on ice. Then, the organs were weighted and transferred to petri dishes with 10mL of PBS. A plunger of a syringe was used to mash the tissue of the spleen and thymus to release cells into the PBS solution. The cell suspensions were filtrated through 40 μm Fisherbrand™ Sterile Cell Strainers (Cat#22-363-547, Fisher Scientific, Hampton, New Hampshire, USA) into 50mL conical centrifuge tubes and centrifuged at 1200 rpm for 5 minutes at 4°C. Pellets were gently re-suspended in 1mL of Red Blood Cell (RBC) Lysis Buffer Hybri-Max™ (Cat#R7757, Sigma-Aldrich, St. Louis, Missouri, USA) at RT and left for 5 minutes to lyse RBCs. Cells were diluted with PBS to a final volume of 50mL. The cells were counted in a Countess II FL Automated Cell Counter (Cat#AMQAF1000, nvitrogen^{TM}) using Trypan Blue Stain 0.4% (Cat#T10282, Invitrogen^{TM}) and Countess Cell Counting Chamber Slides (Cat#C10228, Invitrogen^{TM}).

3.6 Tail Fibroblast (TF) Primary Cell Culture

Whole tails from one-month old mice were collected in PBS on ice and transported to the laboratory for their respective processing. The tails were washed with 75% ethanol in 15mL conical centrifuge tubes for a minute. Immediately, mouse-tail skin was removed, and cut into approximately 4mm^2 pieces with the help of micro-lance 3 Needles Cream 19g x 1.5 (Cat#ND500, Becton Dickinson, Ireland) and carbon steel scalpel blades #22 (Cat#233-0028, Braun, Germany). Tail pieces were treated with 2mg/mL collagenase II (Cat#17101-015, Gibco by life technologies, USA) in Dulbecco's Modified Eagle's Medium high glucose (DMEM) (Cat#D6429, Sigma-Aldrich, United Kingdom) supplemented with 10%

concentration in volume/volume (v/v) Fetal Bovine Serum (FBS) (Cat#F7524, Sigma-Aldrich, USA), 1% v/v L-glutamine solution (200mM) (Cat#G7513, Sigma-Aldrich, United Kingdom) and 1% v/v antibiotics (Penicilin/Streptomycin 10,000 U/mL (Cat#15140-122, Gibco, Life Technologies, USA)) for 24 h [37°C, 5% v/v CO2 incubator]. Next day, the tail pieces were washed with the same medium and gently pipetted up and down around 50 times and filtered through a 40-µm nylon cell strainer (Cat#22-363-547, Fisher Scientific). Filtered samples were centrifuged at 1200 rpm for 5 minutes at RT. Pellets were re-suspended in 10mL of supplemented DMEM and plated in a 10cm culture dish for 24 h [37 °C, 5% v/v CO2 incubator]. At the third day, the medium was discarded and cells were washed with PBS and cultured in 10mL of supplemented DMEM at 37 °C, 5% v/v CO2 incubator.

Cell culture was carried out in a laminar flow bench (KOJAIR®, Vilppula, Finland), which was sterilized with 75% ethanol before and after use. Cells were visualized using an inverted light microscope (Cat#AE31, Motic®, Germany). All plastics were purchased from VWR International (Norway).

3.7 Proliferation assays

Tail fibroblast (TF) cells were plated 5×10^4 cells/mL in triplicate in 6-well plates in supplemented DMEM and counted every 48 hours using 10µL Trypan Blue Stain 0.4% (Cat#T10282, Invitrogen™) mixed with 10µL cells on Countess™ Cell Counting Chamber Slides (Cat#C10228, Invitrogen™), and counted using the Countess™ II FL Automated Cell Counter (Cat#AMQAF1000, Invitrogen™). Every 2 days, the medium was changed. Before counting, medium was discarded then washed with PBS and incubated with Trypsin-EDTA solution (Cat#T3924, Sigma-Aldrich, USA) for 20 minutes at 37°C, 5% v/v CO2 incubator. Fibroblast cells from the second or third passages were used for this assay.

3.8 Telomere - Fluorescence *in situ* hybridization (T-FISH)

Fibroblasts from the second or third passages were used for telomere FISH assay. Fibroblasts were treated with 100ng/mL colcemid (Cat#1512-012, KaryoMAX® Colcemid solution; Gibco) for 6h [73, 76]. Then the cells were incubated in trypsin for 15 minutes and then

combined with the medium collected earlier. Next, cells were lysed in the hypotonic solution (75 mM KCl) at 37 °C for 20 min, then cells were fixed in methanol:acetic acid (3:1), and air dried on slides overnight for the metaphase analysis [73, 78]. Slides were digested with pepsin (1mg/mL) during 10 minutes at 37°C. Subsequently; slides were heated at 80°C for 3 minutes to denature DNA. Finally, telomeres were stained with a Cy3-labeled CCCTAACCCTAACCCTAA probe (PANAGENE, Yuseong-gu, Korea) in 70% formamide (Cat#F-9037, Sigma-Aldrich) at RT for 2 hours, washed, dehydrated and mounted with VECTASHIELD® MOUNTING MEDIUM with DAPI (#H-1200, Vector Laboratories, CA, USA).

Chromosomal breaks were defined by the loss of telomere signal from both sister chromatids, whereas chromatid breaks by no telomere signal at one of the two sister chromatids or a clear lack of DAPI signal in the middle of one chromatid[79]. Metaphase images were captured using a Zeiss Laser TIRF3 microscope equipped with a charge-coupled device (CCD) camera and a 100× objective lens.

3.9 Cell staining for Flow Cytometry

Spleens and thymi were isolated in petri dishes with cold PBS-5% FBS (Cat#F7524, Sigma Life Science). The organs were mashed, filtrated, and centrifuged as previously described (Section 3.5). Pellets were re-suspended in 1mL of RBC lysis buffer Hybri-Max (Cat#R7757, Sigma-Aldrich) and incubated for 5 minutes at RT. Cells were washed with 10mL PBS-5% FBS and centrifuged at 1500 rpm for 5 minutes at 4°C. Pellets were re-suspended in 10ml PBS-5% FBS and a filtered second time through a 40µm cell strainer (Cat#22-363-547, Fisher Scientific). Cells were counted as previously described (Section 3.5).

Cell suspensions were spun down and diluted with PBS-2% FBS to get a final concentration of $2.5x10^7$ cells/mL. Each sample consisted of $2.5x10^6$ cells. The cells were blocked for 15 minutes (RT) with Mouse BD Fc Block™ (Cat#553141, BD Biosciences, New Jersey, USA) diluted 50x in PBS-2% FBS. The samples were then incubated with fluorochrome-conjugated antibodies diluted in PBS-2% FBS for 30 minutes in darkness, 4°C. The cells were washed and spun down (1500rpm, 5 minutes, 4°C) two times with 500µL PBS-2% FBS, before transfer intro Falcon™ Round-bottom polystyrene tubes (Cat#352054, Corning™, New

York, USA). Single-stained CD3/CD19/CD4/CD8 BD™ CompBead Anti-Rat and Anti-Hamster Ig κ particles (Cat#552845, BD Biosciences) were used for compensation. Unstained splenocytes/thymocytes were used as controls. The samples were run in a BD FACSCanto™ flow cytometer using the BD FACSDiva™ software, and the data was further analyzed using the FlowJo® V10 software (FlowJo LLC, New Jersey, USA). Antibodies used in flow cytometry are described in the Table 6.

3.10 *Xlf.Paxx.Trp53* Breeding

Initially, heterozygous *Xlf* mice [53] were crossed with our *Paxx* mouse model[58]. $Xlf^{+/-}$ $Paxx^{+/-}$ mice were then crossed with $Trp53^{+/-}$ mice[77] to obtain suitable genotypes for further breeding. Later, $Xlf^{+/-}Paxx^{+/-}Trp53^{+/-}$ mice were crossed with each other.

This thesis started with the inter-crossing $Xlf^{-/-}$ $Paxx^{+/-}$ $Trp53^{+/-}$ mice.

3.11 Antibodies

Information about antibodies used for Western blot and flow cytometry assays is presented in Tables 5 and 6, respectively.

Table 5: Antibodies used in Western blots. The table summarizes antibody host and target, used dilutions, reference (catalogue number), as well as the antibody supplier.

Antibody	Host, target, type	Dilution	Catalogue #	Supplier
Anti-XLF	Rabbit Anti-Human, polyclonal	1:2000	A300-730A	Bethyl Laboratories, Montgomery, Alabama, USA
Anti-PAXX	Rabbit Anti-Human, polyclonal	1:250	NBP1-94172	NovusBio, Littleton, CO, USA,
Anti-β-actin	Mouse Anti-Human, monoclonal	1:2000	ab8226	Abcam, United Kingdom
Anti-Mouse (HRP-conjugated)	Rabbit Anti-Mouse, polyclonal	1:5000	P0260	Dako Agilent, Santa Clara, USA
Anti-Mouse (HRP-conjugated)	Swine Anti-Rabbit, polyclonal	1:5000	P0399	Dako Agilent, Santa Clara, USA

Table 6: Antibodies used in flow cytometry. The table indicates antibody fluorochrome conjugate, host and target, used dilutions, reference (catalogue number), as well as the antibody supplier.

Antibody	Fluorochrome Conjugate	Host, target, type	Dilution	Catalogue #	Supplier
Anti-CD3ε	APC	Hamster Anti-Mouse	1:100	100312	Biolegend, San Diego, California, USA
Anti-CD4	PE-Cy7	Rat Anti-Mouse, monoclonal	1:100	25-0042-81	Thermo Scientific, San Diego, California, USA
Anti-CD8α	PE-Cy5	Rat Anti-Mouse, monoclonal	1:100	553034	BDBiosciences
Anti-CD19	Pe-Cy7	Rat Anti-Mouse	1:100	115520	Biolegend

3.12 Statistics

GraphPad Prism 8 (La Jolla, California, USA) was used for statistical analysis of body weight, cell counts, spleen weight, thymus weight, and proportions of B and T lymphocytes among the different genotypes. A one-way ANOVA was performed for all groups of variables.

4. RESULTS

4.1 Genotyping

DNA extracted from murine ear samples was used. All mice used for experiments, such as organ isolation, cell counting, Western blot analysis, flow cytometry, T-FISH, and breeding, were characterized genotyping using PCR and gel electrophoresis. *Xlf*$^{-/-}$*Paxx*$^{-/-}$*Trp53*$^{+(-)/-}$ mice were evaluated by PCR twice, before and after the use of the samples. Examples of all PCR assays performed during this project are presented in Figure 10; A) *Xlf* WT allele, B) *Xlf* mutant allele, C) *Paxx* WT and mutant alleles, D) *Ku8*0 WT and mutant alleles, E) *Trp53* WT allele, F) *Trp53* mutant allele, G) *Dna-pkcs* WT allele and H) *Dna-pkcs* mutant allele. For reliability, positive (WT allele), negative (knockout allele), and dH2O controls were used in all PCR assays. Example of *Xlf*$^{-/-}$ *Paxx*$^{-/-}$ *Trp53*$^{+/-}$ mouse identified by PCR is shown in the Figure 11.

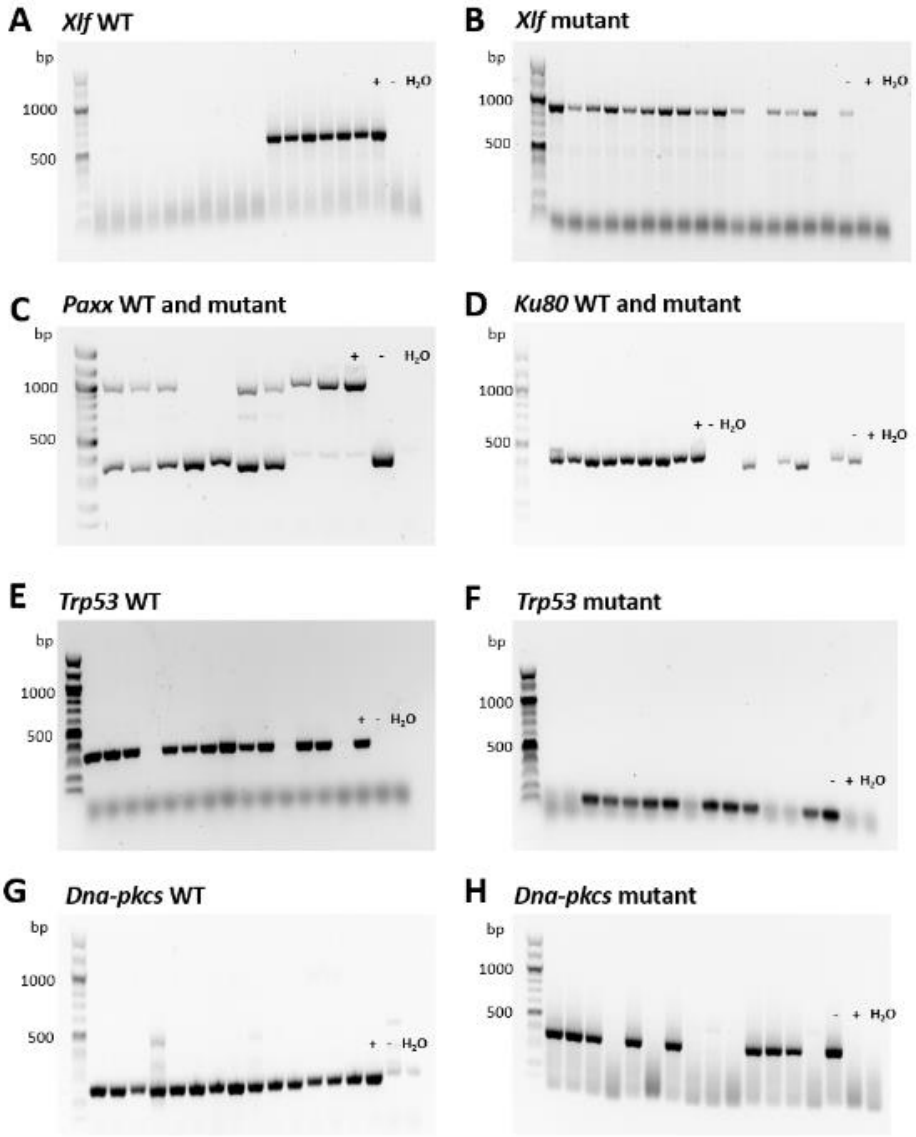

Figure 10: Examples of PCR analysis for *Xlf*, *Paxx*, *Ku80*, *Trp53* and *Dna-pkcs*, with positive ("+", WT allele), negative ("-", mutant allele) and blank samples (H_2O) as controls. **A)** *Xlf* WT. Bands correspond to the *Xlf* WT allele (650bp). **B)** *Xlf* mutant. Bands correspond to the *Xlf* mutant allele (950bp). **C)** *Paxx* WT and mutant. The upper band corresponds to the WT allele (965bp) and the lower band corresponds to the mutant allele (either 329, 312, or 295bp, due to three independent *Paxx* knockout sub-lines used). **D)** *Ku80* WT and mutant. Samples with an amplified WT allele (400bp) are shown to the left, and samples with an amplified mutant allele (320bp) are shown to the right. **E)** *Trp53* WT. Bands correspond to the *Trp53* WT allele (321bp). **F)** *Trp53* mutant. Bands correspond to the *Trp53* mutant allele (150bp). **G)** *Dna-pkcs* WT. Bands correspond to the *Dna-pkcs* WT allele (250bp). **H)** *Dna-pkcs* mutant. Bands correspond to the *Dna-pkcs* mutant allele (427bp).

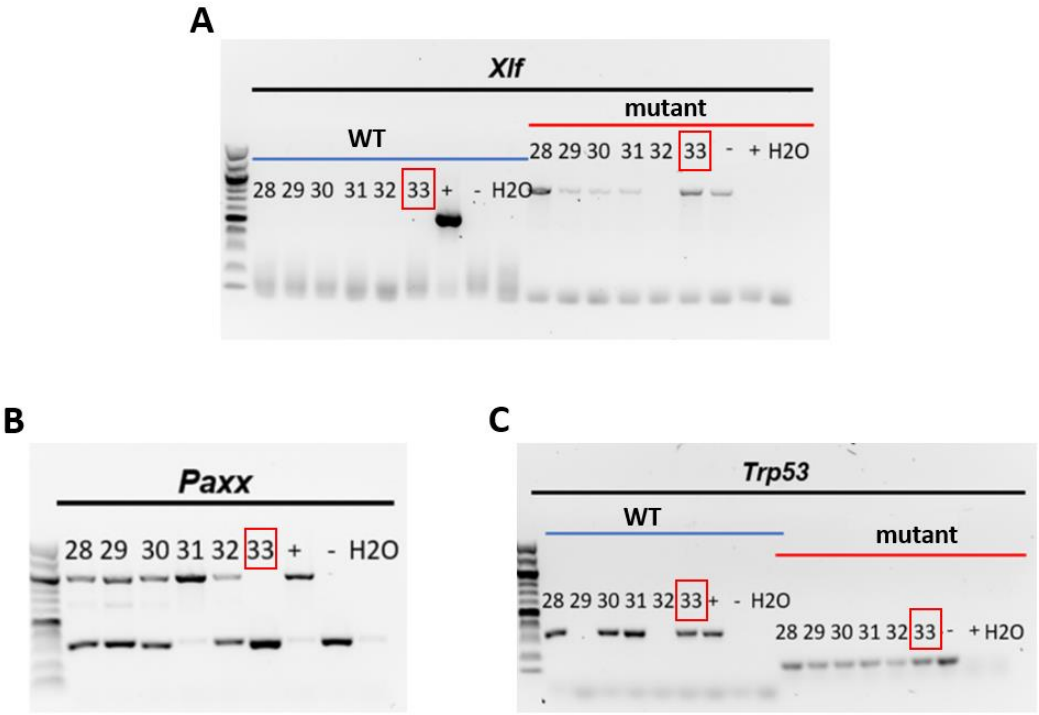

Figure 11: Example of an *Xlf*$^{-/-}$ *Paxx*$^{-/-}$ *Trp53*$^{+/-}$ mouse identified by PCR (Sample number 33 is highlighted in the Figures). **A)** *Xlf* WT and mutant. Sample 33 only has a band corresponding to the mutant allele (genotype *Xlf*$^{-/-}$). **B)** *Paxx* WT and mutant. Sample 33 only has the lower band corresponding to the mutant allele (genotype *Paxx*$^{-/-}$). **C)** *Trp53* WT and mutant. Sample 33 has both bands corresponding to WT and mutant alleles (genotype *Trp53*$^{+/-}$). Sample 33 possesses the genotype *Xlf*$^{-/-}$ *Paxx*$^{-/-}$ *Trp53*$^{+/-}$.

4.2 *Xlf Paxx Trp53* Breeding

According to the previous results, double deficiency of XLF and PAXX leads to an embryonic lethality in mice[56, 57, 59]. I proposed that inactivation of one or two alleles of *Trp53* could rescue the lethality of this combined deficiency in mice. My samples were generated from the crossbreeding of $Xlf^{-/-}$ $Paxx^{+/-}$ $Trp53^{+/-}$ mice.

A total of 120 mice were genotyped. The distribution of the analyzed and expected mice are presented in the Table 7. No $Xlf^{-/-}Paxx^{-/-}$ $Trp53^{+/+}$ mice were found due to the embryonic lethality.

Table 7: Inactivation of *Trp53* rescues synthetic lethality between *Xlf* and *Paxx* in mice. The number of thirty-day-old mice (P30) of the indicated genotypes. Mendelian distribution (Expected) is provided in the third column. Both parents possessed the $Xlf^{-/-}Paxx^{+/-}Trp53^{+/-}$ genotype. In total, 120 mice were screened. Numbers of the genotypes of interest are in red color.

Genotype	Number of offspring, P30	Expected, 1:2:1:2:4:2:1:2:1
$Xlf^{-/-}Paxx^{+/+}Trp53^{+/+}$	9	7,5
$Xlf^{-/-}Paxx^{+/+}Trp53^{+/-}$	21	15
$Xlf^{-/-}Paxx^{+/+}Trp53^{-/-}$	8	7,5
$Xlf^{-/-}Paxx^{+/-}Trp53^{+/+}$	18	15
$Xlf^{-/-}Paxx^{+/-}Trp53^{+/-}$	34	30
$Xlf^{-/-}Paxx^{+/-}Trp53^{-/-}$	10	15
$Xlf^{-/-}Paxx^{-/-}Trp53^{+/+}$	0	7,5
$Xlf^{-/-}Paxx^{-/-}Trp53^{+/-}$	13	15
$Xlf^{-/-}Paxx^{-/-}Trp53^{-/-}$	7	7,5
Total	**120**	**120**

4.3 Protein expression in Tail Fibroblasts (TF)

Samples previously identified by PCR as *Xlf*$^{-/-}$, *Paxx*$^{-/-}$ and *Xlf*$^{-/-}$*Paxx*$^{-/-}$ *Trp53*$^{+(-)/-}$ mice were randomly chosen to confirm the absence of their corresponding proteins by Western blots. Expression of XLF and PAXX proteins was tested using TF primary cell culture extract.

Xlf knockout mice were confirmed by the lack of the XLF (37kDa) band, and *Paxx* knockout mice were confirmed by the lack of the PAXX (22kDa) band. There were neither XLF nor PAXX corresponding bands in *Xlf*$^{-/-}$*Paxx*$^{-/-}$ *Trp53*$^{+(-)/-}$ mice (Figure 12).

β-actin (42kDa) protein was used as a loading control to normalize the protein expression.

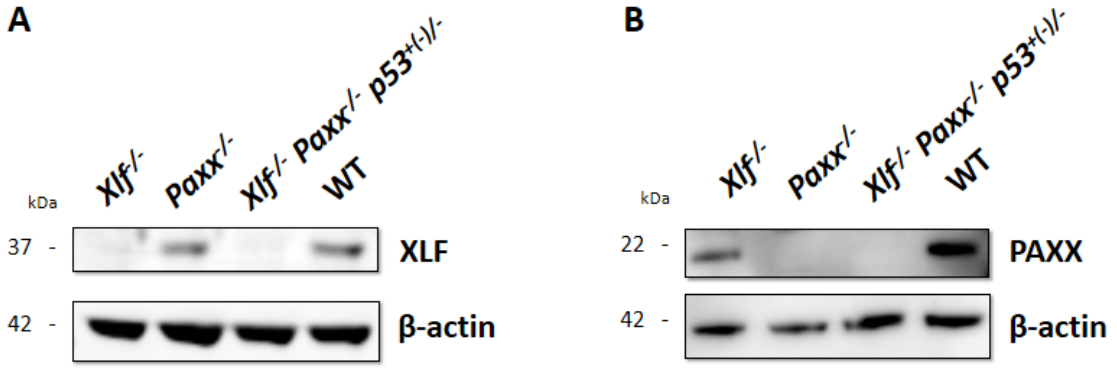

Figure 12: Western blots using anti-XLF (37kDa band) and anti-PAXX (22kDa band) immunoglobulins in *Xlf*$^{-/-}$, *Paxx*$^{-/-}$, *Xlf*$^{-/-}$*Paxx*$^{-/-}$*Trp53*$^{+(-)/-}$ and WT samples. **A)** Detection of XLF in murine tail fibroblasts. **B)** Detection of PAXX in murine tail fibroblasts. Double knockouts were confirmed by the absence of both XLF and PAXX proteins (A and B). 50µg of total cell protein was loaded. β-actin (42kDa) was used as a loading control.

4.4 Growth and Immune system development in *Xlf*$^{-/-}$ *Paxx*$^{-/-}$ *Trp53*$^{+(-)/-}$ mice

A total of 41 mice was used to characterize the body weight, size of spleen, thymus, and the number of cells, which reside in the spleens and thymi among positive controls (samples with WT, *Xlf* and *Paxx* genes, *Xlf*$^{+/+}$ *Paxx*$^{+/+}$) (n=6), *Xlf*$^{-/-}$ (n=16), *Paxx*$^{-/-}$ (n=9) and *Xlf*$^{-/-}$ *Paxx*$^{-/-}$ *Trp53*$^{+(-)/-}$ (n=10) mice. Mice with double knockout of *Xlf* and *Paxx* and partial or total *Trp53* knockout were grouped. No difference among these mice was identified.

Xlf$^{-/-}$ *Paxx*$^{-/-}$ *Trp53*$^{+(-)/-}$ mice were significantly smaller than age-matched *Xlf*$^{+/+}$ *Paxx*$^{+/+}$, and single knockout controls *Xlf*$^{-/-}$ and *Paxx*$^{-/-}$ ($p \leq 0.0001$) (Figure 13 A and B). Furthermore, *Xlf*$^{-/-}$ *Paxx*$^{-/-}$ *Trp53*$^{+(-)/-}$ possessed reduced size of spleens and thymi (Figure 13 C, D and E) and severe lymphocytopenia compared to *Xlf*$^{+/+}$ *Paxx*$^{+/+}$, *Xlf*$^{-/-}$ and *Paxx*$^{-/-}$ controls ($p \leq 0.0001$) (Figure 13 F and G). Apparently, the small quantity of splenocytes and thymocytes corresponds to background levels.

In addition, *Xlf*$^{-/-}$ *Paxx*$^{-/-}$ *Trp53*$^{+(-)/-}$ mice were viable up to 60 days and died for unknown reasons. No tumors were detected in these mice during the indicated period of time. Males and females were pooled together for analysis, and mice were between 4-8 weeks of age when analyzed.

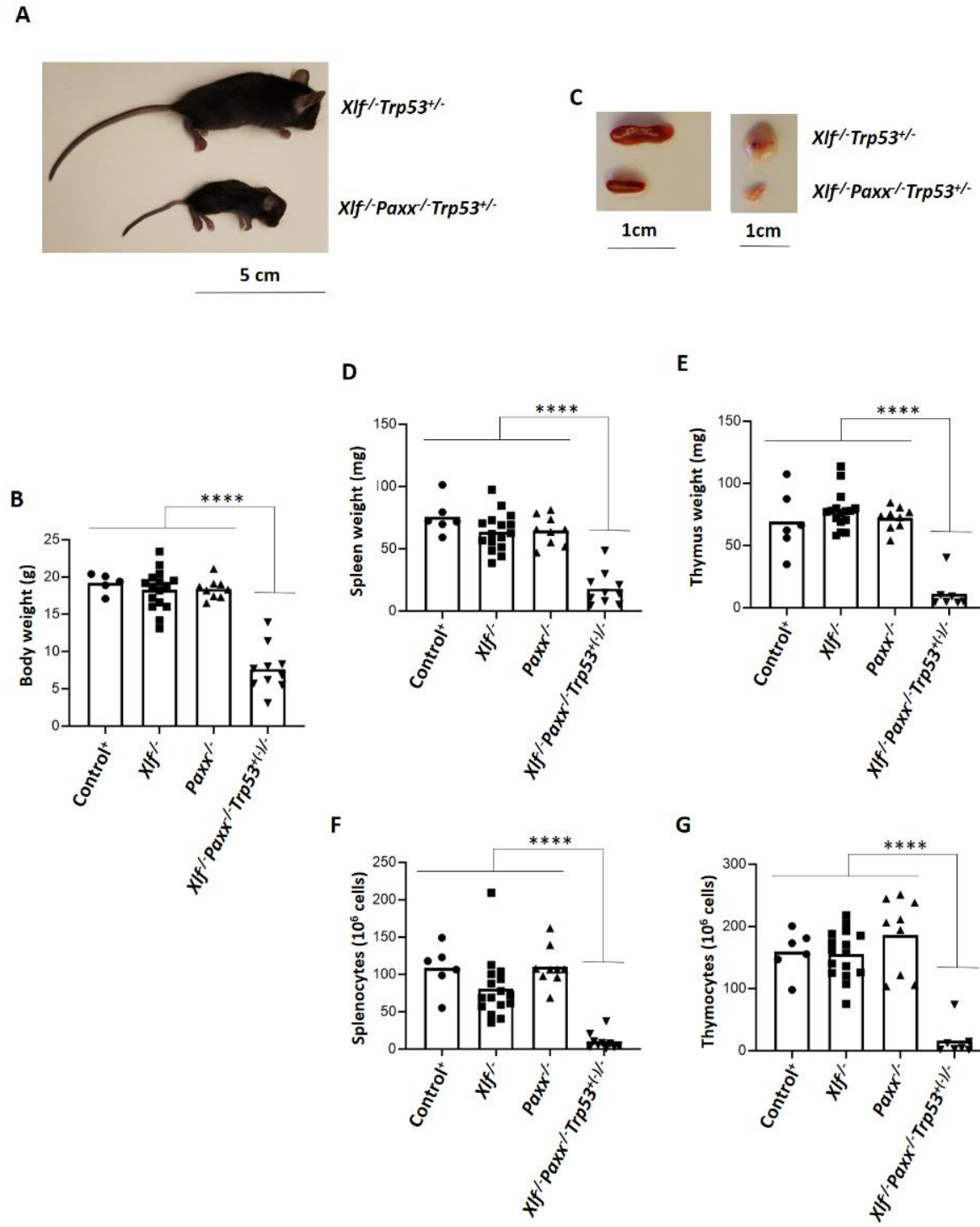

Figure 13: Growth and immune system development of *Xlf*$^{-/-}$ *Paxx*$^{-/-}$ *Trp53*$^{+(-)/-}$ mice. (A) Example of thirty-day-old *Xlf*$^{-/-}$ *Paxx*$^{-/-}$ *Trp53*$^{+/-}$ and *Xlf*$^{-/-}$ *Trp53*$^{+/-}$ female littermates. (B) The average weight of thirty-day-old mice in grams. (C) Spleens (left) and thymi (right) isolated from *Xlf*$^{-/-}$ *Trp53*$^{+/-}$ and *Xlf*$^{-/-}$ *Paxx*$^{-/-}$ *Trp53*$^{+/-}$ mice. The weight of spleens (D) and thymi (E) isolated from thirty-day-old mice of indicated genotypes. Count of splenocytes (F) and thymocytes (G) isolated from thirty-day-old mice of indicated genotypes.

4.5 Frequencies and number of B and T cells in lymphoid organs of *Xlf*$^{-/-}$*Paxx*$^{-/-}$ *Trp53*$^{+/-}$ mice

The splenocytes and thymocytes were analyzed by flow cytometry in order to find if the combined inactivation of *Xlf* and *Paxx* resulted in mice developing B and T lymphocytes.

Xlf$^{-/-}$ *Paxx*$^{-/-}$ *Trp53*$^{+/-}$ (n=3) mice were compared to the single knockouts *Xlf*$^{-/-}$ (n=4) and *Paxx*$^{-/-}$ (n=4), in addition to *Xlf*$^{+/+}$ *Paxx*$^{+/+}$ (n=3) and *Dna-pkcs*$^{-/-}$ mice (n=4) used as controls [68].

Isolated murine splenocytes of indicated genotypes were stained with Anti-C19 and Anti-CD3 antibodies to determine the proportion of B and T cells, respectively. Furthermore, I used Anti-CD4 and Anti-CD8 antibodies to identify CD4^{+} and CD8^{+} single and double positive T cells in the spleens and thymi. The mice used in this analyzes were 5 to 8 weeks old.

CD19^{+} and CD3^{+} (B and T cells, respectively) frequency and count are presented in the Table 8. Examples from flow cytometry analysis of Anti-CD3/Anti-CD19 stained splenocytes are presented in the Figure 14.A. There was significant difference in splenic B and T cells (Figure 14.B.1 and 14.C.1) among *Xlf*$^{-/-}$ *Paxx*$^{-/-}$ *Trp53*$^{+/-}$ compared to controls mice. The total number of B and T cells is shown in the Figure 14.B.2 and 14.C.2.

Table 8: Frequencies (%) and count of B and T cells among *Xlf*$^{+/+}$ *Paxx*$^{+/+}$, , *Xlf*$^{-/-}$, *Paxx*$^{-/-}$, *Xlf*$^{-/-}$*Paxx*$^{-/-}$*Trp53*$^{+/-}$ and *Dna-pkcs*$^{-/-}$ mice analysed by flow cytometry. Molecular markers CD3^{+} and CD19^{+} correspond to T and B cells, respectively. RBCs were lysed prior to flow cytometry analysis, therefore, they were not taken into account.

	Cell frequencies (%)		Number of cells (x10^{6})	
	CD19^{+}	**CD3^{+}**	**CD19^{+}**	**CD3^{+}**
Control^{+}	54,67	14,73	37,65	10,15
Xlf$^{-/-}$	49,75	19,68	24,83	9,82
Paxx$^{-/-}$	57,55	15,2	31,92	8,43
Xlf$^{-/-}$Paxx$^{-/-}$Trp53$^{+/-}$	0,39	5,13	0,04	0,57
Control^{-}	1,19	1,35	0,05	0,05

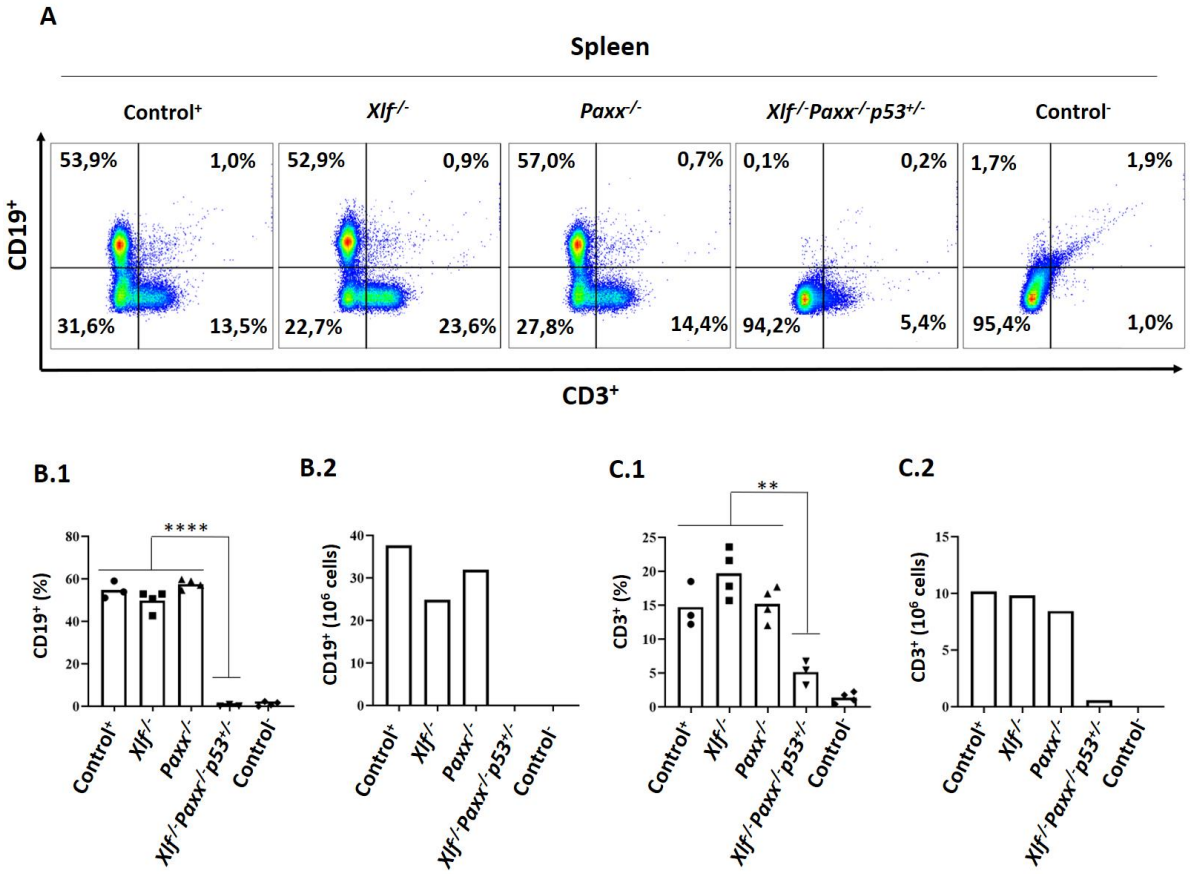

Figure 14: Splenic B and T cells in *Xlf*$^{+/+}$ *Paxx*$^{+/+}$, *Xlf*$^{-/-}$, *Paxx*$^{-/-}$, *Xlf*$^{-/-}$*Paxx*$^{-/-}$*Trp53*$^{+/-}$ and *Dna-pkcs*$^{-/-}$ mice. **A)** Flow cytometry analysis of splenocytes stained with Anti-CD3 (T cell marker) and Anti-CD19 (B cell marker), frequencies (%) are indicated. **B.1)** Comparison in CD19 positive splenocytes (%). **B.2)** Total number of B cells in each genotype. **C.1)** Comparison in CD3 positive splenocytes (%). **C.2)** Total number of T cells in each genotype. *Dna-pkcs*$^{-/-}$ mice were used as negative control. Minimum n=3. Not significant (NS) = $p > 0.05$, * = $p \leq 0.05$, ** = $p \leq 0.01$, *** = $p \leq 0.001$ and **** = $p \leq 0.0001$.

Frequencies and count of $CD4^+$ and $CD8^+$ T splenocytes are presented in the Table 9. A representative Figure from flow cytometry analysis of Anti-CD4/Anti-CD8 stained cells is presented in the Figure 15.A.

Xlf$^{-/-}$ *Paxx*$^{-/-}$ *Trp53*$^{+/-}$ mice showed a significant reduction in the proportion of T helper and T cytotoxic cells compared to *Xlf*$^{+/+}$ *Paxx*$^{+/+}$, *Xlf*$^{-/-}$ and *Paxx*$^{-/-}$ mice (Figure 15.B.1 and 15.C.1). Nevertheless, *Xlf*$^{-/-}$ *Paxx*$^{-/-}$ *Trp53*$^{+/-}$ had a significant increase of $CD8^+$ subset cells compared to negative control mice lacking DNA-PKcs. The number of $CD4^+$ and $CD8^+$ T cells in the spleen is shown in the Figure 15.B.2 and 15.C.2, respectively.

Table 9: Frequencies (%) and number of $CD4^+$, T_H cells and $CD8^+$, T_C cells among *Xlf*$^{+/+}$ *Paxx*$^{+/+}$, *Xlf*$^{-/-}$, *Paxx*$^{-/-}$, *Xlf*$^{-/-}$*Paxx*$^{-/-}$*Trp53*$^{+/-}$ and *Dna-pkcs*$^{-/-}$ mice analysed by flow cytometry. RBCs were lysed prior to flow cytometry analysis, therefore, they were not taken into account.

	Cell frequencies (%)		**Number of cells (x10^6)**	
	CD4$^+$	**CD8$^+$**	**CD4$^+$**	**CD8$^+$**
Control$^+$	14,17	12,97	9,76	8,93
***Xlf*$^{-/-}$**	16,8	14,05	8,38	7,01
***Paxx*$^{-/-}$**	12,9	13,6	7,15	7,54
***Xlf*$^{-/-}$*Paxx*$^{-/-}$*Trp53*$^{+/-}$**	4,62	8,48	0,51	0,94
Control$^-$	2,26	2,67	0,09	0,1

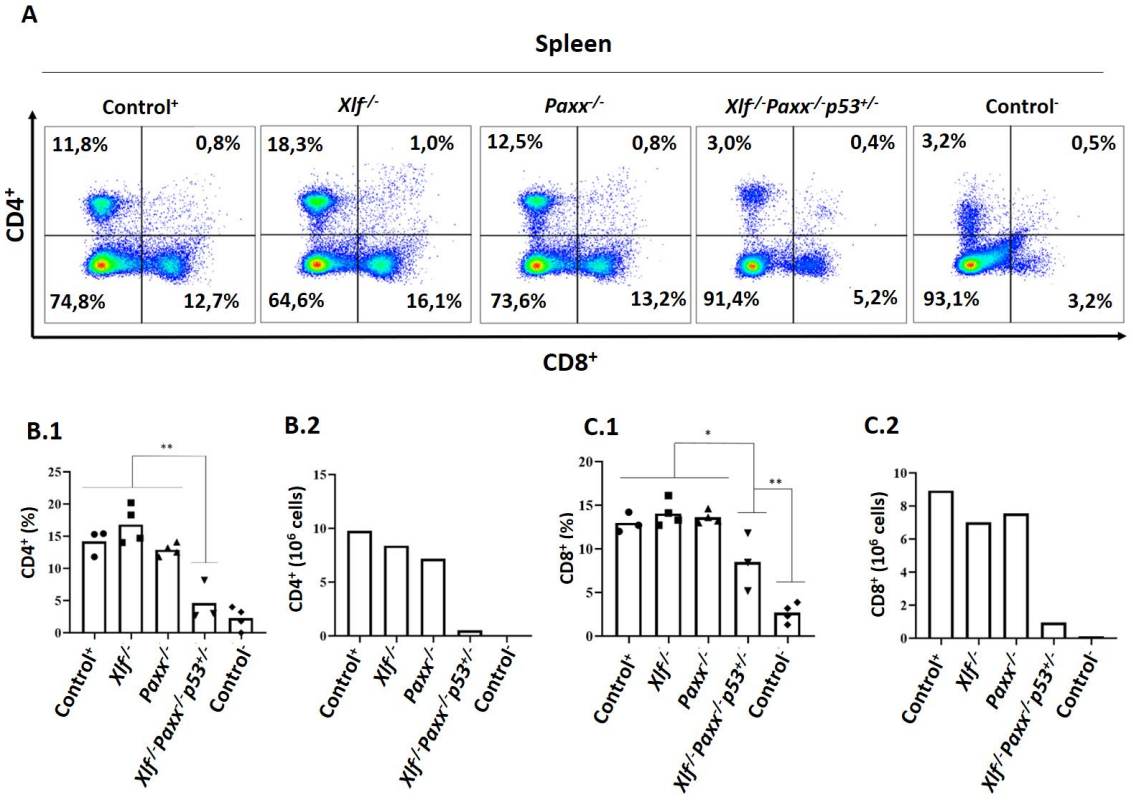

Figure 15: Splenic CD4/CD8 T cells in *Xlf*$^{+/+}$ *Paxx*$^{+/+}$, *Xlf*$^{-/-}$, *Paxx*$^{-/-}$, *Xlf*$^{-/-}$*Paxx*$^{-/-}$*Trp53*$^{+/-}$ and *Dna-pkcs*$^{-/-}$ mice. **A)** Flow cytometry analysis of splenocytes stained with Anti-CD4 (T helper cells) and Anti-CD8 (T cytotoxic), frequencies (%) are indicated. **B.1)** Comparison in CD4 positive splenocytes (%). **B.2)** Total number of T_H cells in each genotype. **C.1)** Comparison in CD8 positive splenocytes (%). **C.2)** Total number of T_C cells in each genotype. T_H: T helper cells. T_C: T cytotoxic cells. *Dna-pkcs*$^{-/-}$ were used as negative control. Minimum n=3. Not significant (NS) = $p > 0.05$, * = $p \leq 0.05$, ** = $p \leq 0.01$, *** = $p \leq 0.001$ and **** = $p \leq 0.0001$.

Thymic cell frequencies and count of $CD4^+CD8^+$, $CD4^+$ and $CD8^+$ T cells, are presented in the Table 10. A representative Figure from flow cytometry analysis of Anti-CD4/Anti-CD8 stained thymocytes is presented in the Figure 16.A.

Xlf$^{-/-}$ *Paxx*$^{-/-}$ *Trp53*$^{+/-}$ mice had a significant reduction in the proportion of CD4 T cells compared to *Xlf*$^{+/+}$ *Paxx*$^{+/+}$, *Xlf*$^{-/-}$ and *Paxx*$^{-/-}$ mice (Figure 16.B.1). However, deficiency for XLF and PAXX resulted in significant increase of T_C cell proportion compared to *Dna-pkcs*$^{-/-}$ mice and no difference compared to *Xlf*$^{+/+}$ *Paxx*$^{+/+}$, *Xlf*$^{-/-}$ and *Paxx*$^{-/-}$ mice (Figure 16.C.1). Additionally, there was a significant reduction of double positive ($CD4^+$ $CD8^+$) thymocytes among *Xlf*$^{-/-}$ *Paxx*$^{-/-}$ *Trp53*$^{+/-}$ compared to *Xlf*$^{+/+}$ *Paxx*$^{+/+}$ and *Paxx*$^{-/-}$ mice. Moreover, mice with combined deficiency for XLF and PAXX possessed a significant increase of DP cells compared to the negative controls lacking DNA-PKcs (Figure 16.D.1). The number of $CD4^+$, $CD8^+$ and $CD4^+$ $CD8^+$ cells is shown in the Figures 16.B.2, 16.C.2 and 16.D.2, respectively.

Table 10: Frequencies (%) and number of thymic DP and SP T cells among *Xlf*$^{+/+}$ *Paxx*$^{+/+}$, *Xlf*$^{-/-}$, *Paxx*$^{-/-}$, *Xlf*$^{-/-}$ *Paxx*$^{-/-}$*Trp53*$^{+/-}$ and *Dna-pkcs*$^{-/-}$ mice analysed by flow cytometry. $CD4^+CD8^+$, double positive T cells; $CD4^+$, T_H cells and $CD8^+$, T_C cells. RBCs were lysed prior to flow cytometry analysis, therefore, they were not taken into account.

	Cell frequencies (%)			**Number of cells (x10^6)**		
	$CD4^+CD8^+$	**$CD4^+$**	**$CD8^+$**	**$CD4^+CD8^+$**	**$CD4^+$**	**$CD8^+$**
Control$^+$	82,2	7,65	4,29	81,71	7,6	4,26
***Xlf*$^{-/-}$**	80,83	8,13	4,85	108,61	10,93	6,51
***Paxx*$^{-/-}$**	83,03	7,54	4,4	111,88	10,16	5,93
***Xlf*$^{-/-}$*Paxx*$^{-/-}$*Trp53*$^{+/-}$**	76,05	2,77	5,45	2,45	0,09	0,18
Control$^-$	1,44	1,75	2,91	0,002	0,003	0,004

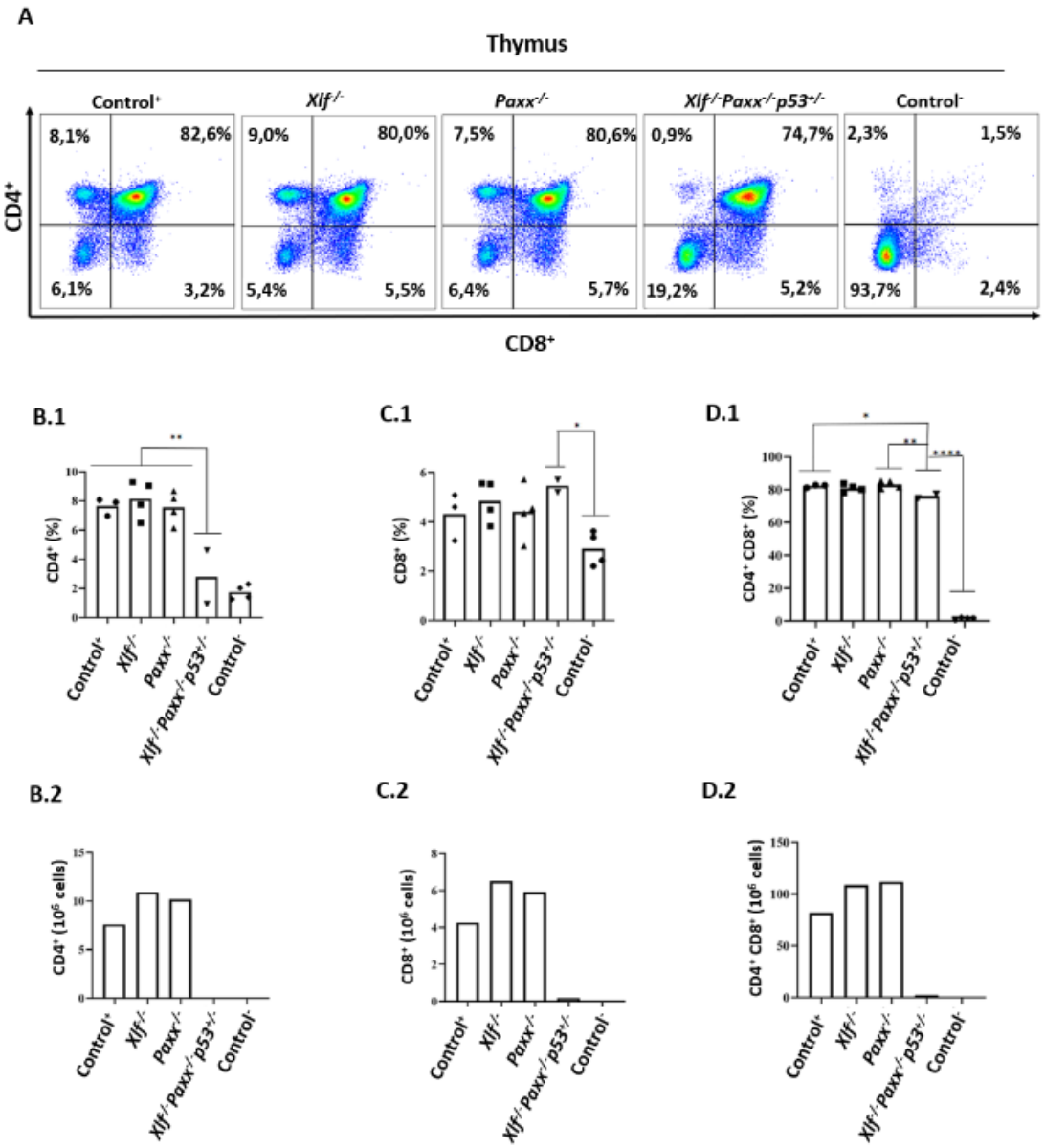

Figure 16: Thymic CD4/CD8 T cells in *Xlf*$^{+/+}$ *Paxx*$^{+/+}$, *Xlf*$^{-/-}$, *Paxx*$^{-/-}$, *Xlf*$^{-/-}$*Paxx*$^{-/-}$*Trp53*$^{+/-}$ and *Dna-pkcs*$^{-/-}$ mice. **A)** Flow cytometry analysis of thymocytes stained with Anti-CD4 (T helper cells) and Anti-CD8 (T cytotoxic). Frequencies of correspondent cell types (%) are indicated. **B.1)** CD4 positive splenocytes (%). **B.2)** Total number of T_H cells in each genotype. **C.1)** CD8 positive splenocytes (%). **C.2)** Total number of T_C cells in each genotype. **D.1)** CD4CD8 double positive splenocytes (%). **D.2)** Total number of double positive (DP) T cells. DP: CD4$^+$CD8$^+$T cells. T_H: T helper cells. T_C: T cytotoxic cells. *Dna-pkcs*$^{-/-}$ were used as negative control. Minimum n=3. Not significant (NS) = $p > 0.05$, * = $p \leq 0.05$, ** = $p \leq 0.01$, *** = $p \leq 0.001$ and **** = $p \leq 0.0001$.

4.6 Proliferation of Tail Fibroblasts (TF)

In order to investigate the proliferative potential of the *Xlf*$^{-/-}$ *Paxx*$^{-/-}$ *Trp53*$^{+/-}$ cells, they were compared against the single knockouts *Xlf*$^{-/-}$ and *Paxx*$^{-/-}$, in addition to *Xlf*$^{+/+}$ *Paxx*$^{+/+}$ controls (same samples as used in the Section 4.5). Three animals of each genotype were selected, and 5×10^4 cells/mL were cultured per sample in triplicate. TFs were counted every 2 days from day 0 until day 6 (Figure 17).

Xlf$^{-/-}$ *Paxx*$^{-/-}$ *Trp53*$^{+/-}$ cells were compared to *Xlf*$^{+/+}$ *Paxx*$^{+/+}$ samples and showed significant difference in the cell proliferation rate. In the second, fourth and sixth day of experiment, the respective p-values were 0,0025; 0,0001 and < 0,0001.

Additionally, *Xlf*$^{-/-}$ *Paxx*$^{-/-}$ *Trp53*$^{+/-}$ mice displayed a significant reduction in number of TF cells compared to *Xlf*$^{-/-}$ mice. In the second, fourth and sixth day of experiment, the respective p-values were 0,0004; 0,0002 and < 0,0001.

Finally, *Xlf*$^{-/-}$ *Paxx*$^{-/-}$ *Trp53*$^{+/-}$ TF proliferation rate was significantly different when compared to *Paxx*$^{-/-}$ TFs. In the second, fourth and sixth days of evaluation, the respective p-values were 0,0013; 0,001 and 0,0003.

A summary of the statistical analysis is provided in the Table 11.

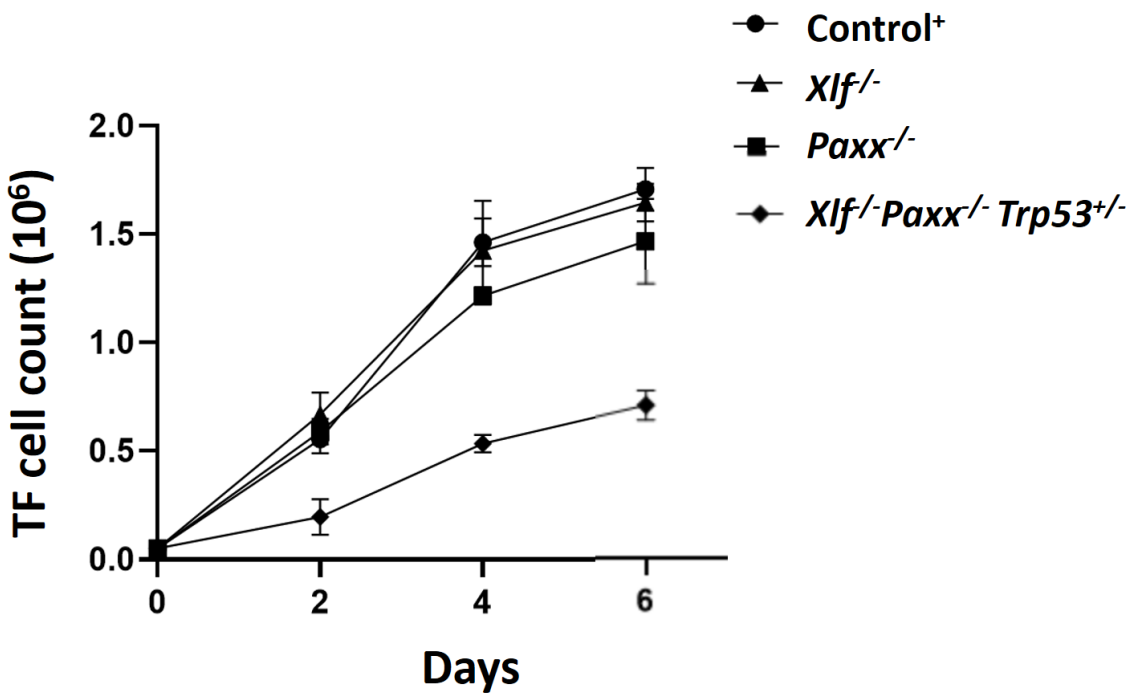

Figure 17: Proliferation of tail fibroblast (TF) cells from *Xlf*$^{+/+}$ *Paxx*$^{+/+}$, *Xlf*$^{-/-}$, *Paxx*$^{-/-}$ *and Xlf*$^{-/-}$ *Paxx*$^{-/-}$ *Trp53*$^{+/-}$ mice. A graph represents a summary of three experiments in triplicates. Control^{+} mice are *Xlf*$^{+/+}$ *Paxx*$^{+/+}$.

Table 11: A summary of the statistical analyzes by one-way ANOVA of TFs proliferation. *Xlf*$^{+/+}$ *Paxx*$^{+/+}$ *vs Xlf*$^{-/-}$ *Paxx*$^{-/-}$ *Trp53*$^{+/-}$, *Xlf*$^{-/-}$ *vs Xlf*$^{-/-}$ *Paxx*$^{-/-}$ *Trp53*$^{+/-}$, and *Paxx*$^{-/-}$ vs *Xlf*$^{-/-}$ *Paxx*$^{-/-}$ *Trp53*$^{+/-}$ mice. Not significant (NS) = $p > 0.05$, * = $p \leq 0.05$, ** = $p \leq 0.01$, *** = $p \leq 0.001$ and **** = $p \leq 0.0001$.

	Control*$^{+}$ *vs ***Xlf*$^{-/-}$ *Paxx*$^{-/-}$ *Trp53*$^{+/-}$**	***Xlf*$^{-/-}$ *vs*** ***Xlf*$^{-/-}$ *Paxx*$^{-/-}$ *Trp53*$^{+/-}$**	***Paxx*$^{-/-}$ *vs*** ***Xlf*$^{-/-}$ *Paxx*$^{-/-}$ *Trp53*$^{+/-}$**
Day 2	**	***	**
Day 4	***	***	***
Day 6	****	***	****

4.7 Genomic stability evaluated by T-FISH

Telomere Fluorescence in situ hybridization (T-FISH) assays was chosen to identify genomic stability at the chromosomal level.

The chromosomes and telomeres were stained with DAPI (a fluorescent stain that binds strongly to adenine–thymine rich regions in DNA) and Cy3-labeled (an orange-fluorescent) CCCTAACCCTAACCCTAA probe, respectively. Chromosomal breaks were defined by the loss of telomere signal from both sister chromatids, whereas chromatid breaks were defined by no telomere signal at one of the two sister chromatids or a clear lack of DAPI signal in the middle of one chromatid (Figure 18).

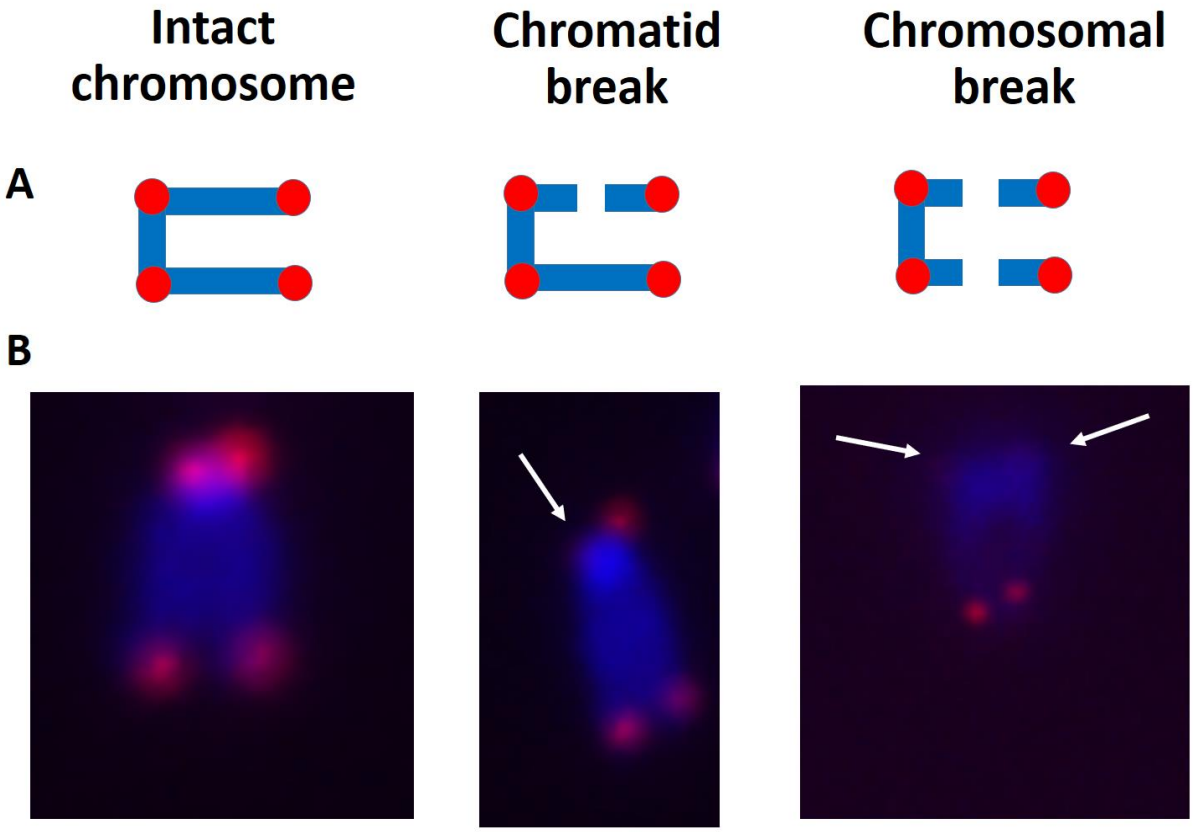

Figure 18: Genomic instability in murine tail fibroblasts. A) Representative scheme of intact and abnormal chromosomes, including chromosome and chromatid breaks. B) Examples from our samples of intact and abnormal chromosomes. Telomeres are in red (Cy3), and DNA is in blue (DAPI).

Xlf$^{-/-}$*Paxx*$^{-/-}$*Trp53*$^{+/-}$ and *Xlf*$^{-/-}$*Paxx*$^{-/-}$*Trp53*$^{-/-}$ TFs were selected in order to investigate the genomic stability using T-FISH assays. However, with the small quantity of TFs after the second or third passages from *Xlf*$^{-/-}$*Paxx*$^{-/-}$*Trp53*$^{+/-}$ samples it was not possible to continue this experiment, whereas, *Xlf*$^{-/-}$*Paxx*$^{-/-}$*Trp53*$^{-/-}$ TFs after second or third passage had enough cells for T-FISH assays.

Furthermore, some changes in the technique were necessary with the purpose of optimizing the method for the future experiments, for instance:

1. Primary tail fibroblasts from mice have to be exposed to trypsin between 15-20 minutes instead of 5 minutes at 37°C to detach from the surface. Or higher concentration of trypsin can be used for shorter time.

2. Five to six petri dishes (1x10^6 cells per dish) in a final volume of 10 ml medium must be used to collect enough samples for analyzes.

3. Increased incubation time in the hypotonic solution (75 mM KCl) at 37 °C from 15 to 20 minutes to obtain more metaphases for analyzes.

All these changes led to improved results.

Table 12: Summary of genomic instability in *Xlf*$^{+/+}$ *Paxx*$^{+/+}$, *Xlf*$^{-/-}$, *Paxx*$^{-/-}$ and *Xlf*$^{-/-}$ *Paxx*$^{-/-}$ *Trp53*$^{-/-}$ mice. Number (n) and proportion (%) of metaphases with detected chromosomal or chromatid breaks in fibroblasts of indicated genotypes are shown.

Genotype	Number of mice	Total Metaphases	Abnormal Metaphases		Chromosomal breaks	Chromatid breaks
		n	n	%	n	n
***Control*$^{+}$**	1	31	2	6,45	2	0
***Xlf*$^{-/-}$**	2	56	7	12,5	9	1
***Paxx*$^{-/-}$**	1	33	3	9,09	5	0
***Xlf*$^{-/-}$*Paxx*$^{-/-}$*Trp53*$^{-/-}$**	2	48	11	22,92	16	3

5. DISCUSSION

5.1 Deficiency for *Trp53* partially rescues embryonic lethality of *Xlf*$^{-/-}$*Paxx*$^{-/-}$ mice

Inactivation of individual *Xlf, Dna-pkcs, Mri* or *Paxx* genes resulted in no obvious defect in the neurodevelopment, nevertheless, combined inactivation of *Xlf* and *Dna-pkcs* (*Xlf*$^{-/-}$ *Dna-pkcs*$^{-/-}$) [73], *Xlf* and *Mri* (*Xlf*$^{-/-}$*Mri*$^{-/-}$) [35] or *Xlf* and *Paxx* (*Xlf*$^{-/-}$*Paxx*$^{-/-}$) [56, 57, 59, 65], resulted in embryonic lethality likely due to severe neuronal apoptosis in murine brain during embryonic development. Core NHEJ knockout mouse models, *Xrcc4*$^{-/-}$ and *Lig4*$^{-/-}$, also possess late embryonic lethality (at day E.15.5). However, deletion or haploinsufficiency for *Trp53* partially rescued embryonic lethality of *Xrcc4*$^{-/-}$ [72, 75] and *Lig4*$^{-/-}$ [71, 80] mice likely due to reduced apoptosis in the central nervous system. Similar results were found in *Xlf*$^{-/-}$ *Dna-pkcs*$^{-/-}$ mice with haploinsufficiency for *Trp53* [65, 76].

It is suggested that XLF plays a role in the neurodevelopment, while it is compensated by other factors, e.g. accessory NHEJ proteins DNA-PKcs, Mri and PAXX. In addition, XLF and PAXX are structural homologues. Moreover, XLF is a conserved protein in all eukaryotes, while PAXX is absent in most invertebrates and in yeast [76], proposing that PAXX has evolved to participate in resolving more complex breaks in higher eukaryotes.

During this project, one hundred and twenty mice from the crossbreeding of *Xlf*$^{+/-}$ *Paxx*$^{+/-}$ *Trp53*$^{+/-}$ mice were genotyped and characterized. No *Xlf*$^{+/-}$ *Paxx*$^{-/-}$ *Trp53*$^{+/+}$ mouse was found. Nevertheless, I discovered that inactivation of one or both alleles of *Trp53* partially rescues the lethality of *Xlf*$^{-/-}$*Paxx*$^{-/-}$ mice, even more interesting, their proportions are similar to the expected mendelian distribution (Table 7 and [65]).

Furthermore, *Xlf*$^{-/-}$ *Paxx*$^{-/-}$ double deficient mice showed no detectable XLF and PAXX protein in tail fibroblasts (Figure 12) confirming the inactivation of both *Xlf* and *Paxx* alleles. TRP53 (p53) expression was not evaluated because its respective antibody was not available.

Additionally, *Xlf*$^{-/-}$ *Paxx*$^{-/-}$ *Trp53*$^{+/-}$ and *Xlf*$^{-/-}$ *Paxx*$^{-/-}$ *Trp53*$^{-/-}$ mice were viable up to 60 days and died for unknown reasons, nonetheless, it is possible that the early lethality of these mice correlates with accelerated aging, and this option requires additional studies.

5.2 Growth and immune system development

PAXX and XLF are not essential for V(D)J recombination due to compensatory mechanisms [53, 55-57, 59, 62, 64, 65, 81], and a combined inactivation of these proteins in mice leads to lethality [56, 57, 59]. *Xlf*$^{-/-}$ mice possess rearranges in V, D, and J segments of pro-B cells and DN thymocytes at nearly WT [52, 53], carrying out to the development of B and T cells, respectively. Furthermore, *Paxx*$^{-/-}$ mice have similar ratios of B and T cell populations when compared to positive controls [56-59]. Similar to my results, where single knockout mice (*Xlf*$^{-/-}$ and *Paxx*$^{-/-}$) show no significant difference among them and when compared to *Xlf*$^{+/+}$ *Paxx*$^{+/+}$ mice.

Inactivation of one or two alleles of *Trp53* results in a partial rescue of lethality in *Xlf*$^{-/-}$*Paxx*$^{-/-}$ mice. It could be due to a reduced cellular apoptosis, which allows postnatal survival. As in the case of *Lig4*$^{-/-}$ *Trp53*$^{+(-)/-}$ and *Xrcc4*$^{-/-}$ *Trp53*$^{+(-)/-}$ mice, where the embryonic lethality is rescued, showing a reduction of the neuronal apoptosis, and premature senescence phenotypes, and no lymphocyte development [75].

Furthermore, our *Xlf*$^{-/-}$*Paxx*$^{-/-}$ *Trp53*$^{+(-)/-}$ deficient mice possess smaller body size, spleen and thymus weight when compared to single knockouts and *Xlf*$^{+/+}$ *Paxx*$^{+/+}$ controls. Additionally, they show a severe reduction of the lymphocytes both in spleens and in thymi. Ku80 deficient mice have a reduction of the body weight by around 50% when compared to WT age and gender-matched mice. Moreover, *Ku80*$^{-/-}$ mice have only some residual cells in spleens and thymi, which correspond to progenitor T cells in the thymi, and other populations of immune cells in the spleens [69]. Data not shown here, but recently published by us, Castaneda-Zegarra, S., *et al*. [65] (Appendix C), that *Xlf*$^{-/-}$ *Paxx*$^{-/-}$ *Trp53*$^{+(-)/-}$ mice have similar body size, spleens/thymi weight and number of splenocytes and thymocytes when compared to *Ku80*$^{-/-}$ mice. It might be due to general DNA repair defect which is similar in these two groups of mice.

5.3 B and T cell frequencies in limphoid organs

B and T, splenocytes and thymocytes from *Xlf*$^{-/-}$ *Paxx*$^{-/-}$ *Trp53*$^{+/-}$ mice were analysed by FACS in order to identify and quantify accurately the frequency and number of cell types. Only three *Xlf*$^{-/-}$ *Paxx*$^{-/-}$ *Trp53*$^{+/-}$ mice were available and no triple knockouts was ready for use at the time of the experiments. To increasing the statistical power, additional *Xlf*$^{-/-}$ *Paxx*$^{-/-}$ *Trp53*$^{+/-}$ mice will be analysed in the future.

Inactivation of one Trp53 allele does not affect the development of lymphocytes in WT mice [39, 71]. It allows us to study an accurate *in vivo* impact of XLF-PAXX deficiency. *Xlf*$^{-/-}$ *Paxx*$^{-/-}$ *Trp53*$^{+/-}$ mice were compared to *Xlf*$^{+/+}$ *Paxx*$^{+/+}$, *Xlf*$^{-/-}$ and *Paxx*$^{-/-}$ controls, as well as *Dna-pkcs*$^{-/-}$ (control^{-}) mice. DNA-PKcs deficient mice have a SCID phenotype and, alike *Ku80*$^{-/-}$, they have just some residual cells in spleens and thymi.

RBCs, mature B and T cells and other immune cells inhabit the spleen. While in the thymus, immature and mature T cells reside. Mature T cells, T helpers (CD4^{+}) and cytotoxic T cells (CD8^{+}) leave from the thymus and pass through the circulation to the lymph nodes or the spleen. In the spleen, B lymphocytes maturate with the assistance of CD4^{+} cells upon interaction with foreign antigens.

Xlf$^{-/-}$ *Paxx*$^{-/-}$ *Trp53*$^{+/-}$ mice possess no B splenocytes, similar to *Dna-pkcs*$^{-/-}$ controls. Although *Xlf*$^{-/-}$ *Paxx*$^{-/-}$ *Trp53*$^{+/-}$ mice did not show difference in splenic T cell frequency when compared to negative control (*Dna-pkcs* deficient) mice, its T-cell frequency is three times higher than in *Dna-pkcs*$^{-/-}$ and three time lower than in *Xlf*$^{+/+}$ *Paxx*$^{+/+}$ mice, respectively. Ouyang, H., *et al*. [82], similarly, showed that it was not possible to identify B cells (CD19^{+}), but there were T cells (CD3^{+}) in *Ku70*$^{-/-}$ splenocytes. Furthermore, *Ku70*$^{-/-}$ mice possessed similar body weight when compared to *Ku80*$^{-/-}$ and their spleens were disproportionately smaller, by 5–10-folds, relative to WT and heterozygous controls. Therefore, *in vivo* XLF and PAXX are required for DNA repair, but possibly there are alternative pathways which would be relevant for T Cell Antigen Receptor Gene Recombination, as it is in the case of *Ku70*$^{-/-}$ mice [74].

Both CD4^{+} and CD8^{+} are present in the spleens of *Xlf*$^{-/-}$ *Paxx*$^{-/-}$ *Trp53*$^{+/-}$ mice, certainly in lower proportion with respect to *Xlf*$^{+/+}$ *Paxx*$^{+/+}$, *Xlf*$^{-/-}$ and *Paxx*$^{-/-}$ samples. However, and

surprisingly, *Xlf*$^{-/-}$ *Paxx*$^{-/-}$ *Trp53*$^{+/-}$ possessed approximately two-thirds of normal CD8^{+} cell frequency. Furthermore, to our surprise, *Xlf*$^{-/-}$ *Paxx*$^{-/-}$ *Trp53*$^{+/-}$ mice had almost normal frequencies of DP T cells (CD4^{+}CD8^{+}) (~ 75%) in the thymi. It implies that DP T cell frequency of *Xlf*$^{-/-}$ *Paxx*$^{-/-}$ *Trp53*$^{+/-}$ samples compared to the rest of genotypes is almost identical, obviating the slight difference in comparison to *Xlf*$^{+/+}$ *Paxx*$^{+/+}$ and *Paxx*$^{-/-}$ mice. This difference might be explained by the small used sample of *Xlf*$^{-/-}$ *Paxx*$^{-/-}$ *Trp53*$^{+/-}$ (n=3) mice.

My data show that in the absence of XLF and PAXX, T cells are able to develop to DP in the thymus, even though the thymus is also disproportionately smaller and contains around 40-fold fewer CD4^{+}CD8^{+} lymphocytes compared to the single knockouts and *Xlf*$^{+/+}$ *Paxx*$^{+/+}$ mice. SP T cells (CD4^{+} or CD8^{+}) are originated from DP T cells in the thymus. The frequency of CD4^{+} T cells in our *Xlf*$^{-/-}$ *Paxx*$^{-/-}$ *Trp53*$^{+/-}$ mice was similar to the negative controls (*Dna-pkcs*-deficient). Nevertheless, strikingly, the CD8^{+} cell proportion was very much similar to the *Xlf*$^{+/+}$ *Paxx*$^{+/+}$, *Xlf*$^{-/-}$ and *Paxx*$^{-/-}$ samples.

Finally, the frequency of CD8^{+} cells in both the spleen and thymus of *Xlf*$^{-/-}$ *Paxx*$^{-/-}$ *Trp53*$^{+/-}$ mice is the double (2:1) regarding to the CD4^{+} cell frequency, even when the normal frequency is the opposite (1:2) in the thymus [25]. It leads us to hypothesize that XLF and PAXX play a role in the development of T lymphocytes from DP T cells to CD4^{+} and CD8^{+} T cells. However, additional experiments are required to make a solid conclusion.

5.4 Proliferation of TFs

Xlf$^{-/-}$ *Paxx*$^{-/-}$ *Trp53*$^{+/-}$ TFs were chosen in order to investigate the cell proliferation, and *Xlf*$^{+/+}$ *Paxx*$^{+/+}$, *Xlf*$^{-/-}$ and *Paxx*$^{-/-}$ cells were used as controls. No *Xlf*$^{-/-}$ *Paxx*$^{-/-}$ *Trp53*$^{-/-}$ mouse was used given that complete inactivation of *Trp53* carries out to a significant increase of cell proliferation due to reduced apoptosis [71, 83, 84].

Xlf$^{-/-}$ *Paxx*$^{-/-}$ *Trp53*$^{+/-}$ TFs show reduced proliferation in the whole experiment compared to single knockouts and positive controls. Likely, in the absence of the accessory factors XLF and PAXX, DSBs cannot be repaired by C-NHEJ and the partial presence of *Trp5*3 would lead a significant proportion of cells to apoptosis. Furthermore, it has been reported that p53 restrains DSBs repair via homologous recombination while promoting non-homologous end joining [85].

No negative controls lacking NHEJ pathway (e.g., Ku70^{-} or Ku80^{-} deficient cells) were available at the time of the experimentation; however, it would be interesting to compare them against XLF-PAXX double deficient TFs.

5.5 Conclusions

We were able to rescue the lethality of XLF-PAXX deficient mice by inactivating one or both alleles of *Trp53*. With this, we confirmed that synthetic lethality between *Xlf* and *Paxx* is *p53*-dependent.

In addition, *Xlf*$^{-/-}$*Paxx*$^{-/-}$*Trp53*$^{+(-)/-}$ mice differ phenotypically from *Xlf*$^{-/-}$ and *Paxx*$^{-/-}$ knockout mice resembling *Ku80*$^{-/-}$ and *Ku70*$^{-/-}$ mice. Moreover, *Xlf*$^{-/-}$*Paxx*$^{-/-}$*Trp53*$^{+(-)/-}$ mice possess reduced body size, spleen and thymus weight, as well as splenocytes and thymocytes count.

Furthermore, flow cytometry analysis of splenocytes and thymocytes isolated from *Xlf*$^{-/-}$*Paxx*$^{-/-}$ *Trp53*$^{+(-)/-}$ mice revealed presence of CD4^{+} and CD8^{+} T cells and an almost normal frequency of CD4^{+}CD8^{+} T cells in the thymi. Nevertheless, and surprisingly, this new mouse model has a frequency of CD8^{+} T cells similar to positive and single knockout controls both in the spleens and thymi. Whereby we can conclude that even when there is a small quantity of SP T cells, CD4^{+}and CD8^{+} T cells are present in less or normal proportion (%), respectively. We also found that *Xlf*$^{-/-}$*Paxx*$^{-/-}$*Trp53*$^{+(-)/-}$ SP T cells can be originated in the thymus and moreover, they can migrate to the spleen.

Additionally, based on our findings, the proliferative power of *Xlf*$^{-/-}$*Paxx*$^{-/-}$*Trp53*$^{+/-}$ cells is significantly less when compared to the single knockouts and WT mice.

Finally, it was possible to optimize the Telomere Fluorescence in situ hybridization (T-FISH) technique, which will be used later to identify genomic stability at the chromosomal level in cells from *Xlf*$^{-/-}$*Paxx*$^{-/-}$*Trp53*$^{+(-)/-}$ and control mice.

5.6 Future directions

With the availability of this new mouse model (*Xlf*$^{-/-}$*Paxx*$^{-/-}$*Trp53*$^{+(-)/-}$), it is possible to characterize mice lacking both XLF and PAXX. In the direction to our obtained results, it would be interesting in a near future to focus on the following aims:

1. To complete a statistically significant sample to evaluate them by T-FISH assay. Around 250 metaphases and n=5 would be a good amount to analyse. It would show us the levels of genomic instability in *Xlf*$^{-/-}$*Paxx*$^{-/-}$*Trp53*$^{+(-)/-}$ mice.

2. To analyse immature B and T cells in the bone marrow of *Xlf*$^{-/-}$*Paxx*$^{-/-}$*Trp53*$^{+(-)/-}$ mice. It would provide us enough data to conclude on the lymphocytic development.

3. A new and interesting approach is to investigate the possible participation of XLF and PAXX in the positive selection from DP T cells ($CD4^+CD8^+$) to SP T cells ($CD4^+$ or $CD8^+$), given our previous results.

6. REFERENCES

1. Schultz, K.T. and F. Grieder, *Structure and function of the immune system.* Toxicol Pathol, 1987. **15**(3): p. 262-4.
2. Yatim, K.M. and F.G. Lakkis, *A brief journey through the immune system.* Clin J Am Soc Nephrol, 2015. **10**(7): p. 1274-81.
3. Parkin, J. and B. Cohen, *An overview of the immune system.* Lancet, 2001. **357**(9270): p. 1777-89.
4. Tosi, M.F., *Innate immune responses to infection.* J Allergy Clin Immunol, 2005. **116**(2): p. 241-9; quiz 250.
5. Dempsey, P.W., S.A. Vaidya, and G. Cheng, *The art of war: Innate and adaptive immune responses.* Cell Mol Life Sci, 2003. **60**(12): p. 2604-21.
6. Kindt, T., R. Goldsby, and B. Osborne, *Kuby Immunology* 6th ed, ed. W.H.F.a. Company. 2006.
7. Bonilla, F.A. and H.C. Oettgen, *Adaptive immunity.* J Allergy Clin Immunol, 2010. **125**(2 Suppl 2): p. S33-40.
8. Boehm, T., *Design principles of adaptive immune systems.* Nat Rev Immunol, 2011. **11**(5): p. 307-17.
9. Fuxa, M. and J.A. Skok, *Transcriptional regulation in early B cell development.* Curr Opin Immunol, 2007. **19**(2): p. 129-36.
10. LeBien, T.W. and T.F. Tedder, *B lymphocytes: how they develop and function.* Blood, 2008. **112**(5): p. 1570-80.
11. Takahama, Y., *Journey through the thymus: stromal guides for T-cell development and selection.* Nat Rev Immunol, 2006. **6**(2): p. 127-35.
12. Hedrick, S.M., *Thymus lineage commitment: a single switch.* Immunity, 2008. **28**(3): p. 297-9.
13. Lin, W.C. and S. Desiderio, *Cell cycle regulation of V(D)J recombination-activating protein RAG-2.* Proc Natl Acad Sci U S A, 1994. **91**(7): p. 2733-7.
14. Roth, D.B., *Restraining the V(D)J recombinase.* Nat Rev Immunol, 2003. **3**(8): p. 656-66.
15. Malu, S., et al., *Role of non-homologous end joining in V(D)J recombination.* Immunol Res, 2012. **54**(1-3): p. 233-46.
16. Schatz, D.G. and Y. Ji, *Recombination centres and the orchestration of V(D)J recombination.* Nat Rev Immunol, 2011. **11**(4): p. 251-63.
17. Montecino-Rodriguez, E. and K. Dorshkind, *B-1 B cell development in the fetus and adult.* Immunity, 2012. **36**(1): p. 13-21.
18. LeBien, T.W., *Fates of human B-cell precursors.* Blood, 2000. **96**(1): p. 9-23.
19. Hardy, R.R., P.W. Kincade, and K. Dorshkind, *The protean nature of cells in the B lymphocyte lineage.* Immunity, 2007. **26**(6): p. 703-14.
20. Pieper, K., B. Grimbacher, and H. Eibel, *B-cell biology and development.* J Allergy Clin Immunol, 2013. **131**(4): p. 959-71.
21. Wang, K., G. Wei, and D. Liu, *CD19: a biomarker for B cell development, lymphoma diagnosis and therapy.* Exp Hematol Oncol, 2012. **1**(1): p. 36.
22. Parham, P., *The Immune System*. 3rd ed. 2009: Garland Science.
23. Holmes, M.L., C. Pridans, and S.L. Nutt, *The regulation of the B-cell gene expression programme by Pax5.* Immunol Cell Biol, 2008. **86**(1): p. 47-53.

24. Matos, T.R., M.A. de Rie, and M.B.M. Teunissen, *Research Techniques Made Simple: High-Throughput Sequencing of the T-Cell Receptor.* J Invest Dermatol, 2017. **137**(6): p. e131-e138.
25. Kuo, T.C. and M.S. Schlissel, *Mechanisms controlling expression of the RAG locus during lymphocyte development.* Curr Opin Immunol, 2009. **21**(2): p. 173-8.
26. Immunology, B.S.f. *T-cell development in thymus.* 2019; Available from: https://www.immunology.org/public-information/bitesized-immunology/immune-development/t-cell-development-in-thymus.
27. Bio-Rad, *Cell frequency by flow citometry.* https://www.bio-rad-antibodies.com/flow-cytometry-cell-frequency.html#%E2%80%8BMurine, 2017.
28. Cannan, W.J. and D.S. Pederson, *Mechanisms and Consequences of Double-Strand DNA Break Formation in Chromatin.* J Cell Physiol, 2016. **231**(1): p. 3-14.
29. Sancar, A., et al., *Molecular mechanisms of mammalian DNA repair and the DNA damage checkpoints.* Annu Rev Biochem, 2004. **73**: p. 39-85.
30. Iyama, T. and D.M. Wilson, 3rd, *DNA repair mechanisms in dividing and non-dividing cells.* DNA Repair (Amst), 2013. **12**(8): p. 620-36.
31. Bohgaki, T., M. Bohgaki, and R. Hakem, *DNA double-strand break signaling and human disorders.* Genome Integr, 2010. **1**(1): p. 15.
32. Haber, J.E., *Recombination: a frank view of exchanges and vice versa.* Curr Opin Cell Biol, 2000. **12**(3): p. 286-92.
33. Ferguson, D.O. and F.W. Alt, *DNA double strand break repair and chromosomal translocation: lessons from animal models.* Oncogene, 2001. **20**(40): p. 5572-9.
34. Takata, M., et al., *Homologous recombination and non-homologous end-joining pathways of DNA double-strand break repair have overlapping roles in the maintenance of chromosomal integrity in vertebrate cells.* EMBO J, 1998. **17**(18): p. 5497-508.
35. Hung, P.J., et al., *MRI Is a DNA Damage Response Adaptor during Classical Non-homologous End Joining.* Mol Cell, 2018. **71**(2): p. 332-342 e8.
36. Rathmell, W.K. and G. Chu, *A DNA end-binding factor involved in double-strand break repair and V(D)J recombination.* Mol Cell Biol, 1994. **14**(7): p. 4741-8.
37. Shibata, A., et al., *Factors determining DNA double-strand break repair pathway choice in G2 phase.* EMBO J, 2011. **30**(6): p. 1079-92.
38. Dobbs, T.A., J.A. Tainer, and S.P. Lees-Miller, *A structural model for regulation of NHEJ by DNA-PKcs autophosphorylation.* DNA Repair (Amst), 2010. **9**(12): p. 1307-14.
39. Jiang, W., et al., *Differential phosphorylation of DNA-PKcs regulates the interplay between end-processing and end-ligation during nonhomologous end-joining.* Mol Cell, 2015. **58**(1): p. 172-85.
40. Ochi, T., et al., *DNA repair. PAXX, a paralog of XRCC4 and XLF, interacts with Ku to promote DNA double-strand break repair.* Science, 2015. **347**(6218): p. 185-188.
41. Cottarel, J., et al., *A noncatalytic function of the ligation complex during nonhomologous end joining.* Journal of Cell Biology, 2013. **200**(2): p. 173-186.
42. Graham, T.G.W., J.C. Walter, and J.J. Loparo, *Two-Stage Synapsis of DNA Ends during Non-homologous End Joining.* Molecular Cell, 2016. **61**(6): p. 850-858.
43. Buck, D., et al., *Cernunnos, a novel nonhomologous end-joining factor, is mutated in human immunodeficiency with microcephaly.* Cell, 2006. **124**(2): p. 287-99.
44. O'Driscoll, M., et al., *DNA ligase IV mutations identified in patients exhibiting developmental delay and immunodeficiency.* Mol Cell, 2001. **8**(6): p. 1175-85.

45. Woodbine, L., et al., *PRKDC mutations in a SCID patient with profound neurological abnormalities.* J Clin Invest, 2013. **123**(7): p. 2969-80.
46. Guo, C., et al., *XRCC4 deficiency in human subjects causes a marked neurological phenotype but no overt immunodeficiency.* J Allergy Clin Immunol, 2015. **136**(4): p. 1007-17.
47. Bennardo, N., et al., *Alternative-NHEJ is a mechanistically distinct pathway of mammalian chromosome break repair.* PLoS Genet, 2008. **4**(6): p. e1000110.
48. Simsek, D. and M. Jasin, *Alternative end-joining is suppressed by the canonical NHEJ component Xrcc4-ligase IV during chromosomal translocation formation.* Nat Struct Mol Biol, 2010. **17**(4): p. 410-6.
49. Chang, H.H.Y., et al., *Non-homologous DNA end joining and alternative pathways to double-strand break repair.* Nat Rev Mol Cell Biol, 2017. **18**(8): p. 495-506.
50. Rulten, S.L. and G.J. Grundy, *Non-homologous end joining: Common interaction sites and exchange of multiple factors in the DNA repair process.* Bioessays, 2017. **39**(3).
51. Callebaut, I., et al., *Cernunnos interacts with the XRCC4 x DNA-ligase IV complex and is homologous to the yeast nonhomologous end-joining factor Nej1.* J Biol Chem, 2006. **281**(20): p. 13857-60.
52. Vera, G., et al., *Cernunnos deficiency reduces thymocyte life span and alters the T cell repertoire in mice and humans.* Mol Cell Biol, 2013. **33**(4): p. 701-11.
53. Li, G., et al., *Lymphocyte-specific compensation for XLF/cernunnos end-joining functions in V(D)J recombination.* Mol Cell, 2008. **31**(5): p. 631-40.
54. Craxton, A., et al., *XLS (c9orf142) is a new component of mammalian DNA double-stranded break repair.* Cell Death Differ, 2015. **22**(6): p. 890-7.
55. Xing, M., et al., *Interactome analysis identifies a new paralogue of XRCC4 in non-homologous end joining DNA repair pathway.* Nat Commun, 2015. **6**: p. 6233.
56. Liu, X., et al., *PAXX promotes KU accumulation at DNA breaks and is essential for end-joining in XLF-deficient mice.* Nat Commun, 2017. **8**: p. 13816.
57. Balmus, G., et al., *Synthetic lethality between PAXX and XLF in mammalian development.* Genes Dev, 2016. **30**(19): p. 2152-2157.
58. Gago-Fuentes, R., et al., *Normal development of mice lacking PAXX, the paralogue of XRCC4 and XLF.* FEBS Open Bio, 2018. **8**(3): p. 426-434.
59. Abramowski, V., et al., *PAXX and Xlf interplay revealed by impaired CNS development and immunodeficiency of double KO mice.* Cell Death Differ, 2018. **25**(2): p. 444-452.
60. Dutrannoy, V., et al., *Clinical variability and novel mutations in the NHEJ1 gene in patients with a Nijmegen breakage syndrome-like phenotype.* Hum Mutat, 2010. **31**(9): p. 1059-68.
61. Recio, M.J., et al., *Extreme Phenotypes With Identical Mutations: Two Patients With Same Non-sense NHEJ1 Homozygous Mutation.* Front Immunol, 2018. **9**: p. 2959.
62. Kumar, V., F.W. Alt, and R.L. Frock, *PAXX and XLF DNA repair factors are functionally redundant in joining DNA breaks in a G1-arrested progenitor B-cell line.* Proc Natl Acad Sci U S A, 2016. **113**(38): p. 10619-24.
63. Dewan, A., et al., *Robust DNA repair in PAXX-deficient mammalian cells.* FEBS Open Bio, 2018. **8**(3): p. 442-448.
64. Lescale, C., et al., *Specific Roles of XRCC4 Paralogs PAXX and XLF during V(D)J Recombination.* Cell Rep, 2016. **16**(11): p. 2967-2979.
65. Castaneda-Zegarra, S., et al., *Synthetic lethality between DNA repair factors Xlf and Paxx is rescued by inactivation of Trp53.* DNA Repair (Amst), 2019. **73**: p. 164-169.

66. Efeyan, A. and M. Serrano, *p53: guardian of the genome and policeman of the oncogenes.* Cell Cycle, 2007. **6**(9): p. 1006-10.
67. Reinhardt, H.C. and B. Schumacher, *The p53 network: cellular and systemic DNA damage responses in aging and cancer.* Trends Genet, 2012. **28**(3): p. 128-36.
68. Gao, Y., et al., *A targeted DNA-PKcs-null mutation reveals DNA-PK-independent functions for KU in V(D)J recombination.* Immunity, 1998. **9**(3): p. 367-76.
69. Nussenzweig, A., et al., *Requirement for Ku80 in growth and immunoglobulin V(D)J recombination.* Nature, 1996. **382**(6591): p. 551-5.
70. Gu, Y., et al., *Growth retardation and leaky SCID phenotype of Ku70-deficient mice.* Immunity, 1997. **7**(5): p. 653-65.
71. Frank, K.M., et al., *DNA ligase IV deficiency in mice leads to defective neurogenesis and embryonic lethality via the p53 pathway.* Mol Cell, 2000. **5**(6): p. 993-1002.
72. Gao, Y., et al., *A critical role for DNA end-joining proteins in both lymphogenesis and neurogenesis.* Cell, 1998. **95**(7): p. 891-902.
73. Oksenych, V., et al., *Functional redundancy between the XLF and DNA-PKcs DNA repair factors in V(D)J recombination and nonhomologous DNA end joining.* Proc Natl Acad Sci U S A, 2013. **110**(6): p. 2234-9.
74. Rooney, S., et al., *Artemis-independent functions of DNA-dependent protein kinase in Ig heavy chain class switch recombination and development.* Proc Natl Acad Sci U S A, 2005. **102**(7): p. 2471-5.
75. Gao, Y., et al., *Interplay of p53 and DNA-repair protein XRCC4 in tumorigenesis, genomic stability and development.* Nature, 2000. **404**(6780): p. 897-900.
76. Xing, M., et al., *Synthetic lethality between murine DNA repair factors XLF and DNA-PKcs is rescued by inactivation of Ku70.* DNA Repair (Amst), 2017. **57**: p. 133-138.
77. Jacks, T., et al., *Tumor spectrum analysis in p53-mutant mice.* Curr Biol, 1994. **4**(1): p. 1-7.
78. Franco, S., et al., *H2AX prevents DNA breaks from progressing to chromosome breaks and translocations.* Mol Cell, 2006. **21**(2): p. 201-14.
79. Oksenych, V., et al., *Functional redundancy between repair factor XLF and damage response mediator 53BP1 in V(D)J recombination and DNA repair.* Proc Natl Acad Sci U S A, 2012. **109**(7): p. 2455-60.
80. Frank, K.M., et al., *Late embryonic lethality and impaired V(D)J recombination in mice lacking DNA ligase IV.* Nature, 1998. **396**(6707): p. 173-7.
81. Hung, P.J., et al., *Deficiency of XLF and PAXX prevents DNA double-strand break repair by non-homologous end joining in lymphocytes.* Cell Cycle, 2017. **16**(3): p. 286-295.
82. Ouyang, H., et al., *Ku70 is required for DNA repair but not for T cell antigen receptor gene recombination In vivo.* J Exp Med, 1997. **186**(6): p. 921-9.
83. Guevara, N.V., et al., *The absence of p53 accelerates atherosclerosis by increasing cell proliferation in vivo.* Nat Med, 1999. **5**(3): p. 335-9.
84. Jones, S.N., et al., *The tumorigenic potential and cell growth characteristics of p53-deficient cells are equivalent in the presence or absence of Mdm2.* Proc Natl Acad Sci U S A, 1996. **93**(24): p. 14106-11.
85. Moureau, S., et al., *A role for the p53 tumour suppressor in regulating the balance between homologous recombination and non-homologous end joining.* Open Biol, 2016. **6**(9).

APPENDIXES

Appendix A: Primer sequences and expected WT and mutant amplicons of *Paxx, Xlf, Trp53, Ku80* and *Dna-pkcs*.

Primers	Sequence	Amplicons
Paxx Forward	ACAGAGGGTGGTGACTCAGACAATGG	WT 965bp Mutant 329, 312, 295bp
Paxx Reverse	GGAAATGCTATTAGAACCACTGCCACG	
Xlf WT	CATGTTGGCTCTGCGAATAGA	WT 650bp Mutant 950bp
Xlf Mutant	CTGTCTTGTGGGCATAGTAGGC	
Xlf Common	GAGCTCGGATATGAGCGCTCAG	
Trp53 WT	AGGCTTAGAGGTGCAAGCTG	WT 321bp Mutant 150bp
Trp53 Mutant	CAGCCTCTGTTCCACATACACT	
Trp53 Common	TGGATGGTGGTATACTCAGAGC	
Ku80 WT	AGCTTCCACCCTCTAGAGAT	WT 400bp Mutant 320bp
Ku80 Mutant	TAAAGCGCATGCTCCAGACT	
Ku80 Common	ATTGTGATGTGTGGGACACG	
Dna-pkcs WT	GAAAAAGTCTATGAGCTCCTGGGAG	WT 250bp Mutant 427bp
Dna-pkcs Mutant	ACGTAACTCCTCTTCAGACCT	
Dna-pkcs Common	CCCTCCAGACAGCCAGCTAAGACAGG	

Appendix B: PCR Programs

A

***Paxx* (WT/Mutant)**			
Step	**Time**	**Temperature (°C)**	**Cycles**
Initial denaturation	2 min	94	1
Denaturation	30 sec	94	30
Annealing	45 sec	68	
Elongation	1 min	72	
Final extension	5 min	72	1
Hold	∞	4	

B

***Xlf* (WT/Mutant)**			
Step	**Time**	**Temperature (°C)**	**Cycles**
Initial denaturation	3 min	95	1
Denaturation	30 sec	95	40
Annealing & elongation	1 min	62	
Final extension	5 min	68	1
Hold	∞	4	

C

***Trp53* (WT/Mutant)**			
Step	**Time**	**Temperature (°C)**	**Cycles**
Initial denaturation	2 min	95	1
Denaturation	30 sec	95	30
Annealing	30 sec	67	
Elongation	20 sec	72	
Final extension	5 min	72	1
Hold	∞	4	

D

***Ku80* (WT/Mutant)**			
Step	**Time**	**Temperature (°C)**	**Cycles**
Initial denaturation	2 min	94	1
Denaturation	20 sec	94	40
Annealing	15 sec	61	
Elongation	40 sec	72	
Final extension	5 min	72	1
Hold	∞	4	

E

***Dna-pkcs* WT**			
Step	**Time**	**Temperature (°C)**	**Cycles**
Initial denaturation	3 min	94	1
Denaturation	45 sec	94	30
Annealing	45 sec	66	
Elongation	1 min	72	
Final extension	5 min	72	1
Hold	∞	4	

F

***Dna-pkcs* Mutant**			
Step	**Time**	**Temperature (°C)**	**Cycles**
Initial denaturation	3 min	94	1
Denaturation	45 sec	94	40
Annealing	45 sec	59,5	
Elongation	1 min	72	
Final extension	5 min	72	1
Hold	∞	4	

Appendix C: Scientific article (1st author) published this year, 2019, about my master thesis.

DNA Repair 73 (2019) 164–169

Contents lists available at ScienceDirect

DNA Repair

journal homepage: www.elsevier.com/locate/dnarepair

Synthetic lethality between DNA repair factors *Xlf* and *Paxx* is rescued by inactivation of *Trp53*

Sergio Castañeda-Zegarra[a,b,c], Mengtan Xing[a,b], Raquel Gago-Fuentes[a,b], Siri Sæterstad[a,b], Valentyn Oksenych[a,b,d,*]

[a] Department of Clinical and Molecular Medicine, Norwegian University of Science and Technology, Laboratory Center, Erling Skjalgssons gate 1, 7491, Trondheim, Norway
[b] St. Olavs Hospital, Trondheim University Hospital, Clinic of Medicine, Postboks 3250 Sluppen, 7006, Trondheim, Norway
[c] Department of Biomedicine, University of Bergen, Bergen, Norway
[d] Department of Biosciences and Nutrition, Karolinska Institutet, Huddinge, Sweden

ARTICLE INFO

Keywords:
Synthetic lethality
Genetic interaction
SCID
B lymphocyte
Cernunnos

ABSTRACT

Non-homologous end joining (NHEJ) is a DNA repair pathway that senses, processes and ligates DNA double-strand breaks (DSBs) throughout the cell cycle. During NHEJ, core Ku70 and Ku80 subunits bind DSBs as a heterodimer and promote further recruitment of accessory factors (e.g., PAXX, Mri, DNA-PKcs, Artemis) and downstream core subunits XRCC4 and DNA ligase 4 (Lig4). Inactivation of *Ku70* or *Ku80* genes in mice results in immunodeficiency and high levels of genomic instability; deletion of individual *Dna-pkcs*, *Xlf*, *Paxx* or *Mri* genes results in viable mice with no or modest DNA repair defects. However, combined inactivation of either *Xlf* and *Dna-pkcs*, or *Xlf* and *Paxx*, or *Xlf* and *Mri*, leads to synthetic lethality in mice, which correlates with increased levels of apoptosis in the central nervous system. Here, we demonstrated that inactivation of pro-apoptotic factor *Trp*53 rescues embryonic lethality of $Xlf^{-/-}Paxx^{-/-}$ and $Xlf^{-/-}Dna\text{-}pkcs^{-/-}$ double knockout mice. Moreover, combined inactivation of *Paxx* and *Dna-pkcs* results in live-born fertile $Paxx^{-/-}Dna\text{-}pkcs^{-/-}$ mice indistinguishable from $Dna\text{-}pkcs^{-/-}$ knockout controls.